Science Reports, Institute of Geoscience, University of Tsukuba,
Section A, (Geographical Sciences), Vol. 23, 2002, pp. 1-40.

Rates of Rock Property Changes due to Weathering: Sandstone Gravel in Fluvial Terrace Deposits in the Miyazaki Plain

Ken-ichi NISHIYAMA

Abstract

Temporal changes in colour, mineralogical, chemical, physical and mechanical properties due to weathering during 350,000 years were examined using sandstone gravel in fluvial terrace deposits with a known emergence time which were distributed in the Miyazaki Plain, South Kyushu. The time between the age of each terrace formation (20-, 70-, 90-, 110-, 120-, 250- and 350-ka) and the present was assumed to be the weathering period. Naked-eye observation shows that (1) weathering rind is mostly not found in whole cut sections and (2) younger gravels (70-, 90-, 110-, 120-ka gravel) and older ones (250- and 350-ka gravel) have a yellowish and reddish coloured, respectively.

Main results of the measurements are as follows: (1) according to observation of mineral texture in thin sections, pore volume increases with increasing weathering period, and connected pores formed in the matrix of sandstone, (2) matrix minerals such as illite, kaolinite and chlorite gradually decrease with increasing weathering period, (3) the a^*-value of colour index increases during 120- to 350-ka and b^*-value increases during 0- to 120-ka, (4) visible diffuse reflectance increases in the zone of long wavelength in older gravels, (5) chemical compositions of SiO_2, K_2O, MgO, Na_2O and CaO gradually decrease with increasing weathering period, while $FeO+Fe_2O_3$ and Al_2O_3 are constant during 350 ka, (6) X-ray CT images are homogeneity in the whole of cross section, and weathering rinds cannot be recognised, (7) *CT*-value decreases with increasing weathering period, (8) specific gravity decreases, but effective porosity increases with increasing weathering period, (9) pore radius and pore volume increase with increasing weathering period, especially pore radius increases rapidly during 110- to 120-ka, (10) specific surface area changes with a constant rate during 350 ka, (11) the results of EDS analysis show that Fe concentrates in the matrix of sandstone, and Si and alkali elements such as K and Na leach with increasing weathering period, and (12) rock strength index decreases drastically during 0- to 120-ka.

Combining above results suggest that (1) increasing of pores in gravel with increasing weathering period is derived from leaching of matrix, i.e., decreasing SiO_2 and alkali elements; (2) iron concentration and formation of goehtite and hematite occur in older gravels; (3) connected pores formed owing to leaching of matrix minerals; (4) distribution of pores is homogeneity in the whole of gravel, then weathering rind cannot be recognised; and (5) while pore size and pore volume increase with increasing weathering period, owing to winding pores are rare, changing rate of specific surface area and chemical weathering indices are constant during 350 ka. The second finding is compatible to the evidence that the colour of the older gravel changes colour from yellowish to reddish. In summary, leaching of matrix and increasing pore volume plays a major role in the weathering of sandstone.

INTRODUCTION

Weathering influences the processes and rates of landform development. The study of these processes and rates of rock weathering is, therefore, important for geomorphology. Moreover, problems concerning rock weathering are widespread and affect many other research fields in earth sciences and engineering such as mineralogy, geochemistry, soil science, engineering geology, petroleum geology and civil engineering.

Clarifying the rates and mechanism of sandstone weathering is necessary for researchers working in the earth sciences because sandstone is widely distributed in earth's land surface. Previous studies on the weathering mechanism and rates of sandstone have been limited in number (e.g., Bell, 1978; Chigira, 1988, 1991; Chigira and Sone, 1988; Pentecost, 1991; Urusay et al., 1994; Halsey, 1996; Butenuth et al., 1998; Tugrul and Zarif, 1998; Bell and Linsay, 1999; Paichik, 1999), and research involving measuring rock properties as a way of researching the weathering process has been even more limited (Chigira, 1988, 1991; Chigira and Sone, 1988).

Studies on the changing rates of rock properties due to weathering have been limited in number (Kimiya, 1975 b; Crook and Gliespie, 1986; Yusa et al., 1991; Oguchi et al. 1994, 1999; Suzuki and Hachinohe, 1995; Oguchi and Matsukura, 1996, 1999; White et al., 1998; Hachinohe et al., 1999 a, b), because of difficulties in estimating weathering periods. In order to solve the rates and mechanism of sandstone weathering, this study investigates the rock properties of sandstone gravel taken from terrace deposits in a series of dated fluvial terraces in the Miyazaki Plain, south Kyushu. The rates of long-term weathering are estimated based on the assumption that the weathering period is equal to the period between the age of emergence of these terraces and the present. This study can discuss the changes in rock properties due to weathering during 350 ka.

The measured sandstone properties include the following: (1) rock texture and mineralogical properties (observation of thin sections, mineral compositions using X-ray diffraction and visible diffuse spectra), (2) colours, (3) physical properties (effective porosity, pore-size distribution, specific surface area, permeability and internal pore structure of rocks using X-ray CT), (4) chemical properties (chemical compositions using X-ray fluorescence analysis and distributions of chemical elements using energy dispersive X-ray spectrometry) and (5) mechanical properties (point load strength). Using these data, the relationships between rock properties and weathering period in an attempt to clarify the rates and mechanism of weathering of sandstone gravel.

GEOMORPHOLOGOCAL AND GEOLOGICAL SETTING OF THE MIYAZAKI PLAIN

General Setting of the Miyazaki Plain

The Miyazaki Plain is located along the Pacific coast of Southeast Kyushu (Fig. 1). On the northwest side of the Miyazaki Plain lie the Kyushu Mountains, which are chiefly composed of Mesozoic to Cenozoic sedimentary complex. The plain has an area of ca. 900 km^2 and altitudes from 0 to 200 m above sea level. Three large rivers (Omaru, Hitotsuse and Ohyodo) flow across the plain from northwest to southeast. Many terrace surfaces are developed in the Miyazaki Plain, as described later.

Quaternary Stratigraphy and Tephrochronology of the Miyazaki Plain

The Miyazaki Plain (Fig. 1) has the best-developed middle to late Quaternary deposits in Kyushu. The stratigraphy of this plain has been investigated in previous studies (e.g., Otsuka, 1930 a, b; Endo, 1968; Kino et al., 1984; Nagaoka, 1984, 1986; Endo and Suzuki, 1986; Kimura et al., 1991). Recently, the stratigraphy of marine sediments and terrace deposits were discussed by Nagaoka et al. (1998, 1999), and

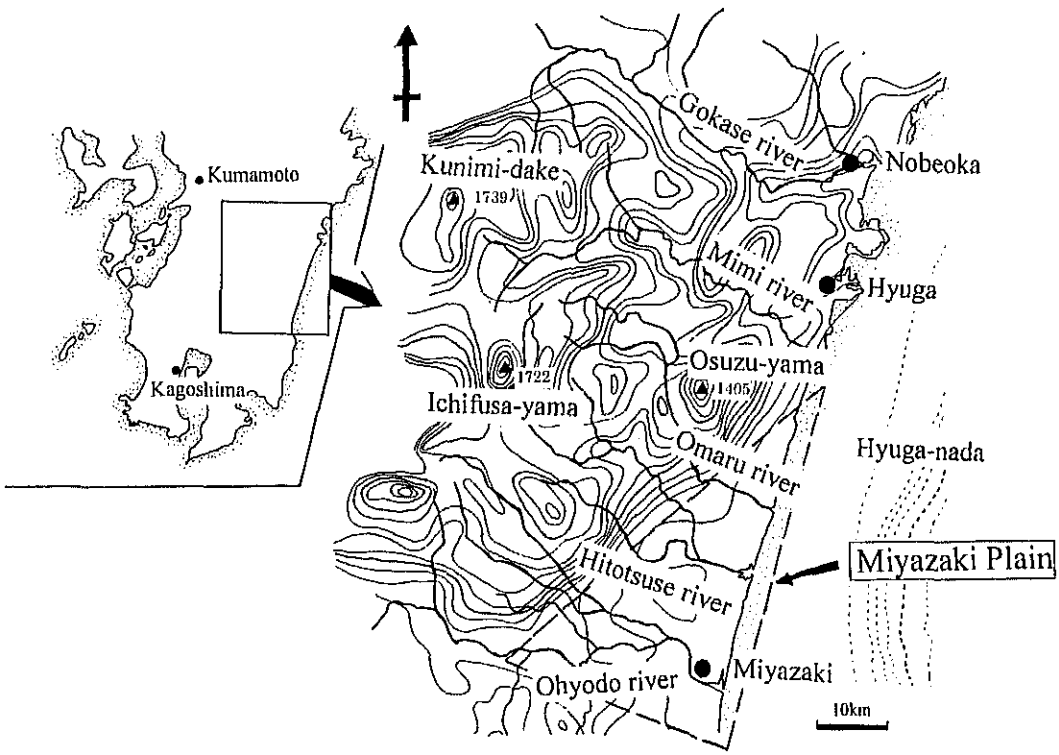

Fig. 1 Summit level map around the Miyazaki Plain (after Endo and Suzuki, 1986). Contour interval is 100m.

this study used their classification of marine sediments and terrace deposits.

The terrace surfaces in the Miyazaki Plain are classified into two groups, the middle to lower terrace group and the higher terrace group. The middle to lower terrace group contains the following terraces in order from the youngest to the oldest: Fukadoshi surface, Ikatsuno surface, Saitobaru surface, Nyutabaru surface, Baba surface and Sanzaibaru surface. The higher terrace group contains the following terraces in order from youngest to oldest: Chausubaru surface, Urushinobaru surface, Kukino surface, Higashibaru surface and Shiibaru surface (Figs. 2 and 3). In these terraces, Sanzaibaru surface has a marine origin, while the other surfaces have a fluvial origin. Geological sections of these terraces are shown in Fig. 4. All of the terrace deposits unconformably cover the Neogene Miyazaki Group and/or the Paleogene Shimanto Supergroup.

The thick tephra layers overlying the terrace surfaces are subdivided into the younger and the older groups based on geologic age (Table 1). The younger and the older tephra groups were deposited in the late Pleistocene and the middle Pleistocene, respectively (Machida and Arai, 1992). The older tephra groups contain many marker tephra layers, such as, from youngest to oldest, Ata-Torihama (Ata-Th), Kakuto (Kkt), Kobayashi-Kasamori (Kb-Ks) and Hiwaki (Hwk). The younger tephra also contains many marker tephra layers, such as, beginning with the youngest, Kikai-Akahoya (K-Ah), Kirishima-Kobayashi (Kr-Kb), Aira-Tn (AT), Kirishima-Awaokoshi (Kr-Aw), Kirishima-Iwaokoshi (Kr-Iw), Aira-Iwato (A-Iw), Aso-4, Aira-Fukuyama (A-Fk), Kikai-Tozurahara (K-Tz), Ata and Aso-3. Each type of tephra was identified by naked-eye observation,

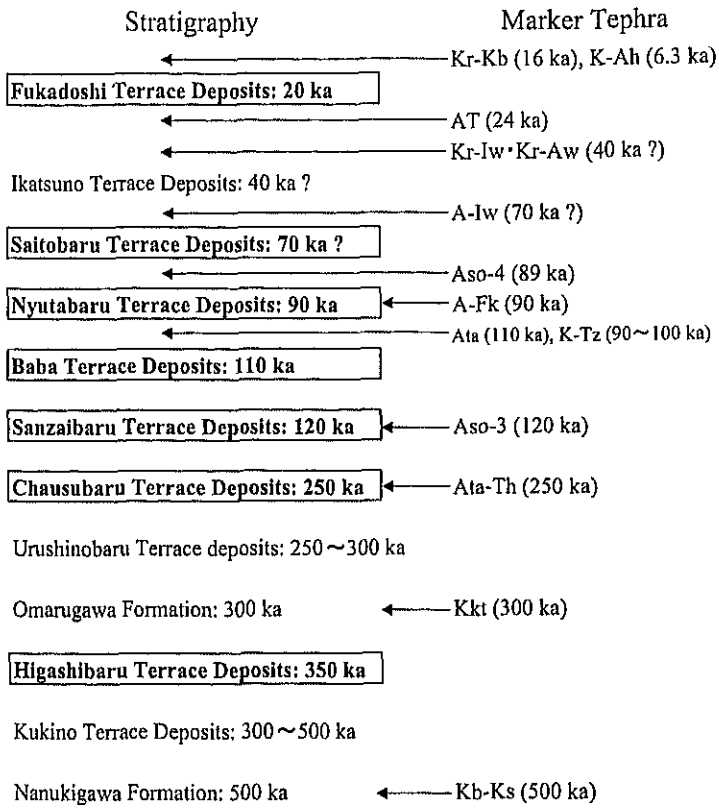

Fig. 2 Stratigraphy of the middle to late Pleistocene sediments in the Miyazaki Plain.

microscope observation and measurements of the refractive index of pyroxene, hornblende and volcanic glass. The younger tephra group covers the middle to lower terraces in the late Pleistocene, and the older tephra group covers the higher terrace group in the middle Pleistocene.

Quaternary marine sediments distributed in the Miyazaki Plain were named the Tohriyamahama formation by Otsuka (1930 a). Since Otsuka's assertion, opinions are diverse concerning the stratigraphic position of the middle Pleistocene marine sediments (Otsuka, 1930 a; Endo, 1968, Nagaoka, 1986; Endo and Suzuki, 1986). Quaternary marine sediments are divided into three formations by marker tephra, the Nanukigawa formation, the Omarugawa (Hedagawa) formation and the Sanzaibaru formation (Nagaoka et al., 1998). The Nanukigawa and the Omarugawa formations contain as marker tephras the Kb-Ks and the Kkt, respectively. The Sanzaibaru formation contain as marker tephras the Aso-3, and formed the Sanzaibaru surface, while the other formations are overlain unconformably by the Chausubaru terrace deposits, the Sanzaibaru formation and the Ikatsuno terrace deposits.

Geological Features of Sampling Points and Rock Samples for Analysis

The locations of the eight rock sampling sites are shown in Figs. 3 and 4. All sampling points are directly covered with tephra layers (Fig. 5), except for the recent river floodplain. All sampling points at each site are above the groundwater level to avoid the possible influence of groundwater levels on weathering (Nishiyama et al., 1999).

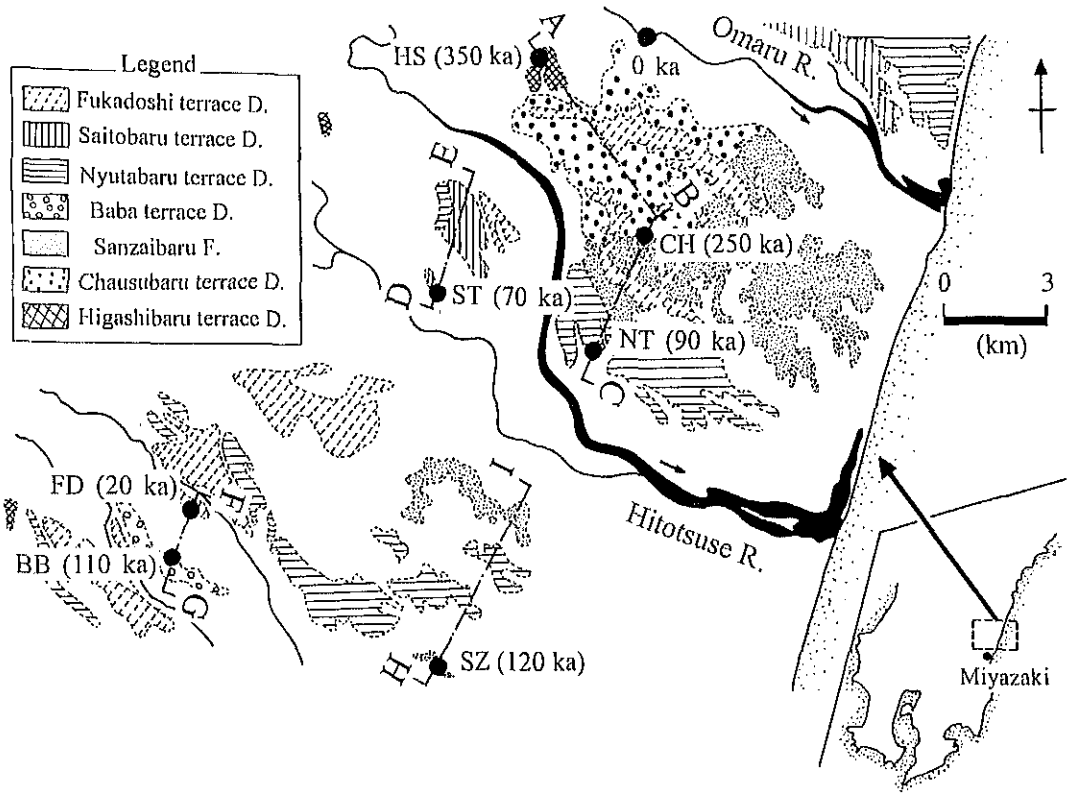

Fig. 3 Geomorphological map in the middle part of the Miyazaki Plain and sampling points.

Figure 6 lists the characteristics of the rock based on naked-eye observations of cutting surfaces. All examined sandstones belong to the Paleogene Shimanto Supergroup. All sandstone gravel samples are fine- to medium-grain wacke-type with smaller amounts of rock fragments. About 20 samples of rounded sandstone cobbles and pebbles were taken from each sampling point. The characteristics of the eight sampling sites and sandstone gravel sample taken from the sampling sites are as follows:

(1) *Recent river floodplain (0-ka rocks)*: The sampling point is located on a gravel bar of river floodplain in the Omaru River (Fig. 3). The gravel taken from this site is not visibly weathered. The cutting surface of this gravel shows that it is dark gray coloured and has no weathering rind. This gravel is hard, and sounds made by hammer blows to it are clear.

(2) *Fukadoshi terrace deposits (20-ka rocks)*: Gravely deposits of this sampling point are almost directly covered by the tephra Kr-Kb and black humic soils (the so-called 'Kuroboku'). The covering tephra layer is about 1 m thick (Fig. 5). The gravel taken from this point is slightly weathered, and its colour is light gray. This gravel has no weathering rind. It is hard, and sounds made by hammer blows to it are clear.

(3) *Saitobaru terrace deposits (70-ka rocks)*: Gravely deposits of the sampling point are almost directly covered by the tephra A-Iw. The covered tephra layer is about 3 m thick (Fig. 5). The gravel taken from this site is slightly weathered, and its colour is light gray. This gravel is hard, and sounds made by hammer blows to it are a little dim.

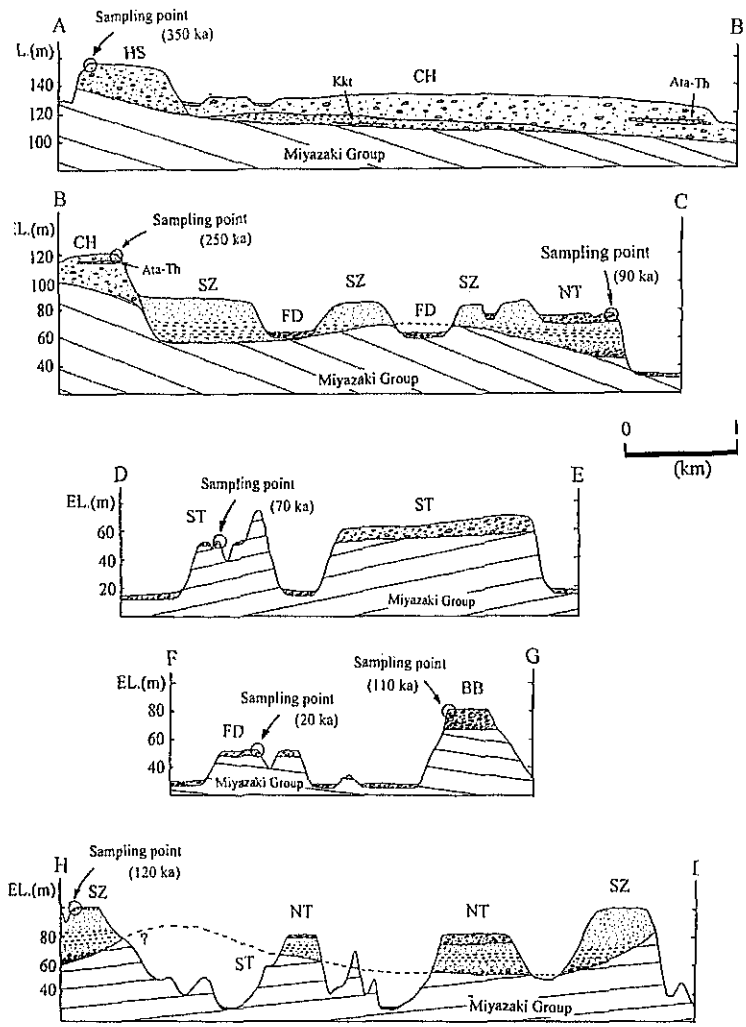

Fig. 4 Geological sections. Profile lines are shown in Fig. 3.

(4) *Nyutabaru terrace deposits (90-ka rocks)*: Gravely deposits of this sampling point are almost directly covered by the tephra A-Fk. The covered tephra layer is about 7 m thick (Fig. 5). The gravel taken from this site is slightly weathered, and its colour is light gray to brown. This gravel is brittle, and sounds made by hammer blows to it are somewhat dim.

(5) *Baba terrace deposits (110-ka rocks)*: Gravely deposits of this sampling point are almost directly covered by the tephra Ata. The covered tephra layer is about 7 m thick (Fig. 5). This gravel is slightly weathered, and its colour is brown. This gravel is brittle, and sounds made by hammer blows to it are dim.

(6) *Sanzaibaru terrace deposits (120-ka rocks)*: Gravely deposits of this sampling point are almost directly covered by the tephra K-Tz. The covered tephra layer is about 6 m thick (Fig. 5). The gravely deposits are correlated with the non-marine upper member of the Sanzaibaru formation. The gravel taken from this site is strongly weathered, and its colour is brown to reddish brown. This gravel is brittle, and sounds made by hammer blows to it are dim.

Table 1 Tephra layers distributed in the Miyazaki Plain

	Name	Symbol	Age (ka)	Mode of occurrence
Younger tephra group	Kikai-Akahoya	K-Ah	6.3	Ash fall
	Kirishima-Kobayashi	Kr-Kb	16	Pumice fall
	Aira-Tn	AT	24	Ash fall
	Kirishima-Awaokoshi	Kr-Aw	30～40？	Pumice fall
	Kirishima-Iwaokoshi	Kr-Iw	30～40？	Pumice fall
	Aira-Iwato	A-Iw	50～70？	Ash fall
	Aso-4	Aso-4	89	Ash fall and pyroclastic flow
	Aira-Fukuyama	A-Fk	90～100？	Ash fall
	Kikai-Tozurahara	K-Tz	90～100？	Ash fall
	Ata	Ata	110	Ash fall and pyroclastic flow
	Aso-3	Aso-3	120	Ash fall
Older tephra group	Ata-Torihama	Ata-Th	230～250	Ash fall and pyroclastic flow
	Kakuto	Kkt	300～340	Ash fall and pyroclastic flow
	Kobayashi-Kasamori	Kb-Ks	500	Ash fall and pyroclastic flow
	Hiwaki	Hwk	600	Ash fall and pyroclastic flow

(7) *Chausubaru terrace deposits (250-ka rocks)*: Gravely deposits of this sampling point are almost directly covered by the tephra Kr-Iw. The covered tephra layer is about 4 m thick (Fig. 5). Deposits contain the tephra Ata-Th in the middle part. The gravel taken from this site is strongly weathered, and its colour is reddish brown. This gravel is brittle, and sounds made by hammer blows to it are dim.

(8) *Higashibaru terrace deposits (350-ka rocks)*: Gravely deposits of this sampling point are almost directly covered by the tephra Ata-Th. The covered tephra layer is about 4 m thick (Fig. 5). The gravel taken from this site is strongly weathered, and it is reddish in colour. This gravel is brittle, and sounds made by hammer blows to it are dim.

ANALYSIS AND RESULTS

Rock Texture and Mineralogical Properties

The petrographical, mineralogical and chemical properties of sandstone in Kyushu Shimanto terrene have been described by Okada (1977), Teraoka (1977; 1979), Kimura et al. (1991) and Teraoka et al. (1995; 1999). These papers show that the sandstone is mostly fine- to medium-grained wacke-type, which consists of phenocrysts of quartz and feldspar (plagioclase and alkali feldspar) with smaller amounts of chert, rock fragments, heavy minerals and mica. The matrix in sandstone mostly consists of clay minerals. Okada (1977) recognised a small amount of calcite cements in the matrix.

Microscope observation was carried out using three rock samples taken from each sampling site. Figure 7 shows representative photomicrographs of sandstone in the thin sections. Most of the rock samples are fine-grained wacke-type, consisting of phenocrysts of quartz and plagioclase, and clay and iron minerals in the matrix. Although the appearance of quartz phenocrysts has not changed as the weathering period has grown longer, plagioclase has been decomposed during the past 350 ka. Matrix minerals have also decomposed, as shown by the fact that the thin sections of matrix become increasingly unclear

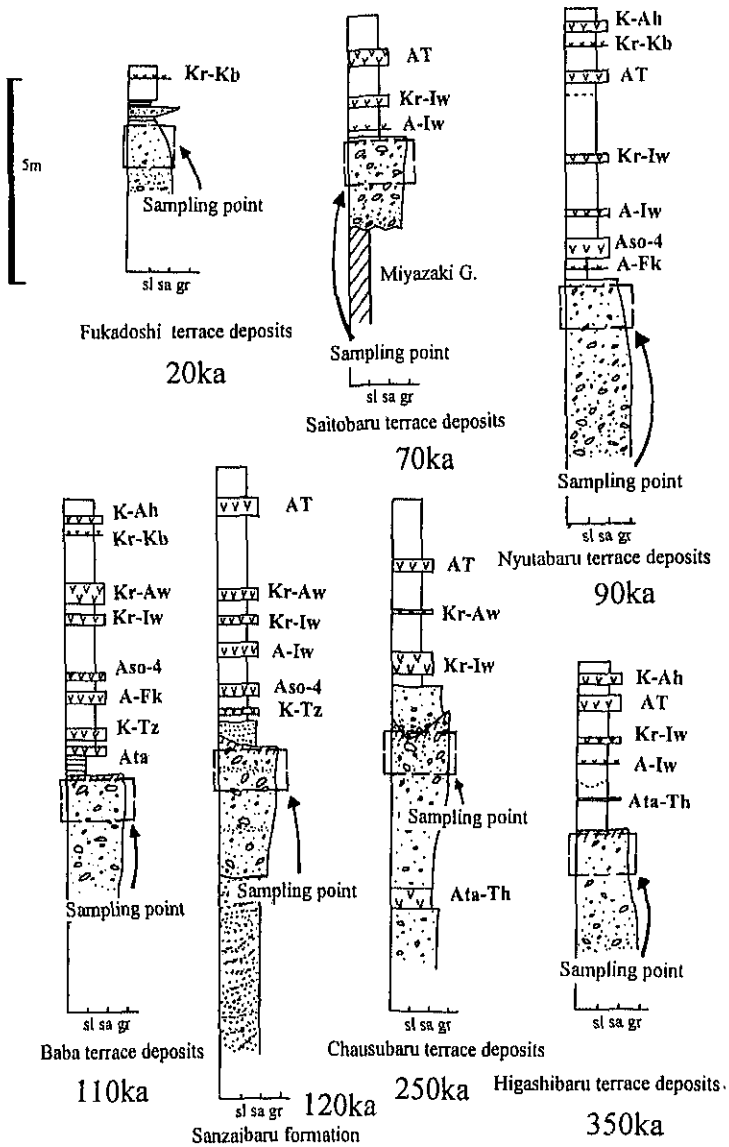

Fig. 5 Columnar sections of sampling points.

as the weathering period increases, while iron minerals with a diameter of about 10 to 100 μm have gradually concentrated in matrix during 350 ka. Small particles of iron minerals surround sand grains, and big particles of iron minerals in 350-ka rocks fill the pore space produced by leaching of feldspar grains.

Observations of pores in thin sections have been included in previous studies (e.g., Nishiyama et al., 1992; Takahashi et al., 1992; Suzuki and Takahashi, 1994; Hirono and Nakashima, 2000). Since pores are filled with petropoxy resin, the area of pores can be recognised as a yellowish zone in matrix, as shown in Fig. 7. Pores are stretched and connected from the outer parts to the inner parts.

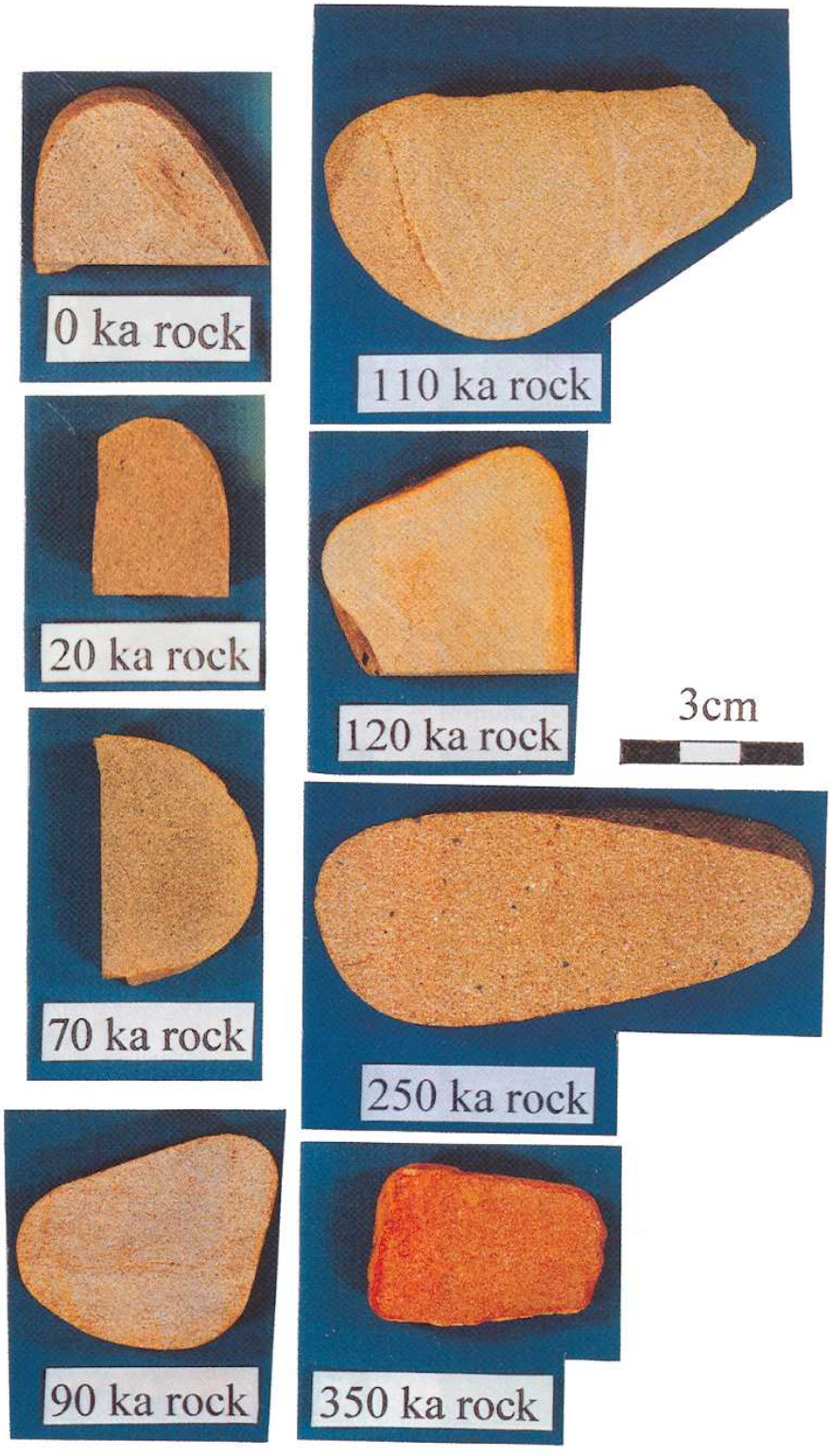

Fig. 6 Cutting surface of sandstone gravel.

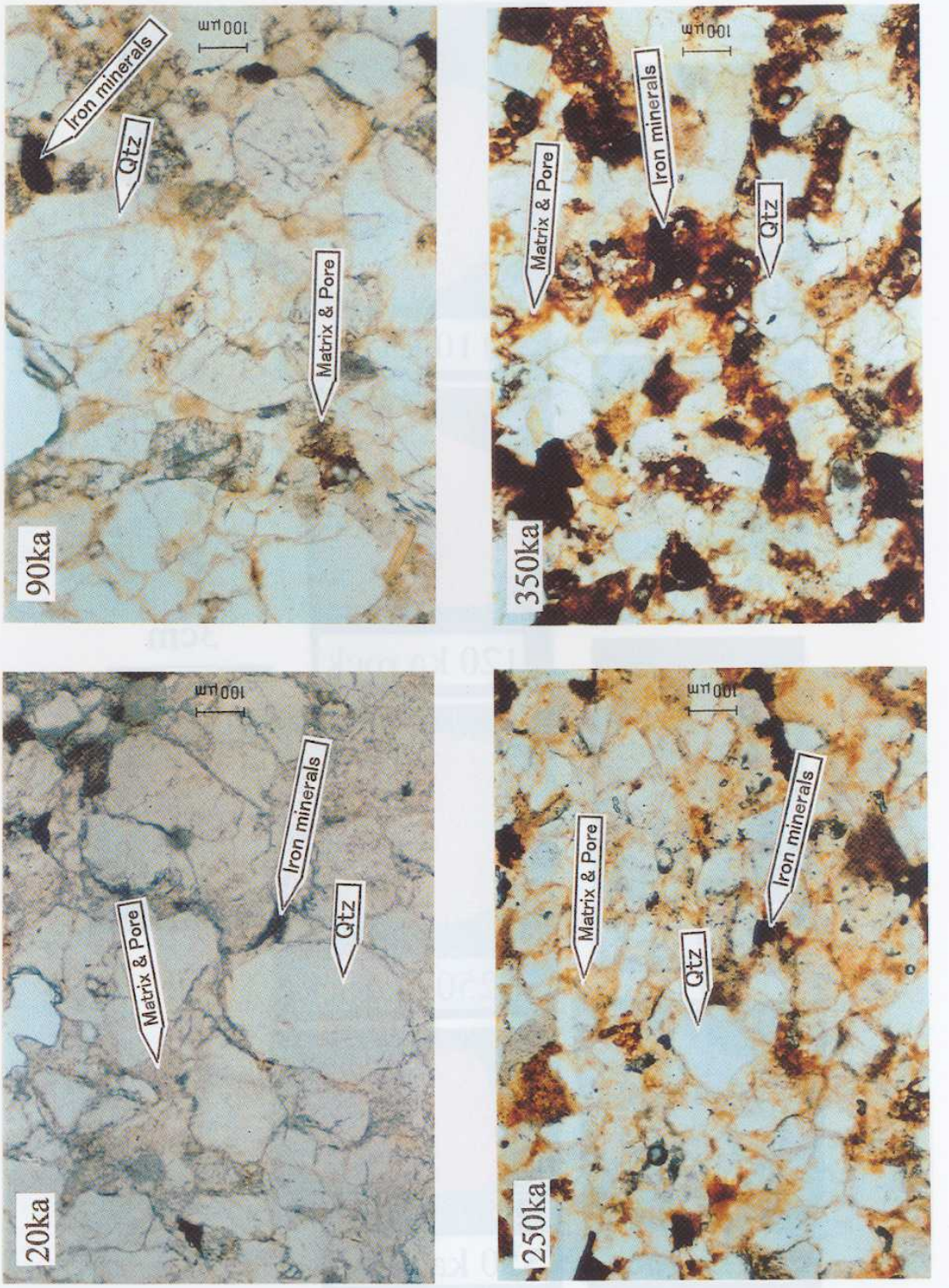

Fig. 7 Photomicrographs of sandstone in thin section (open nicols).

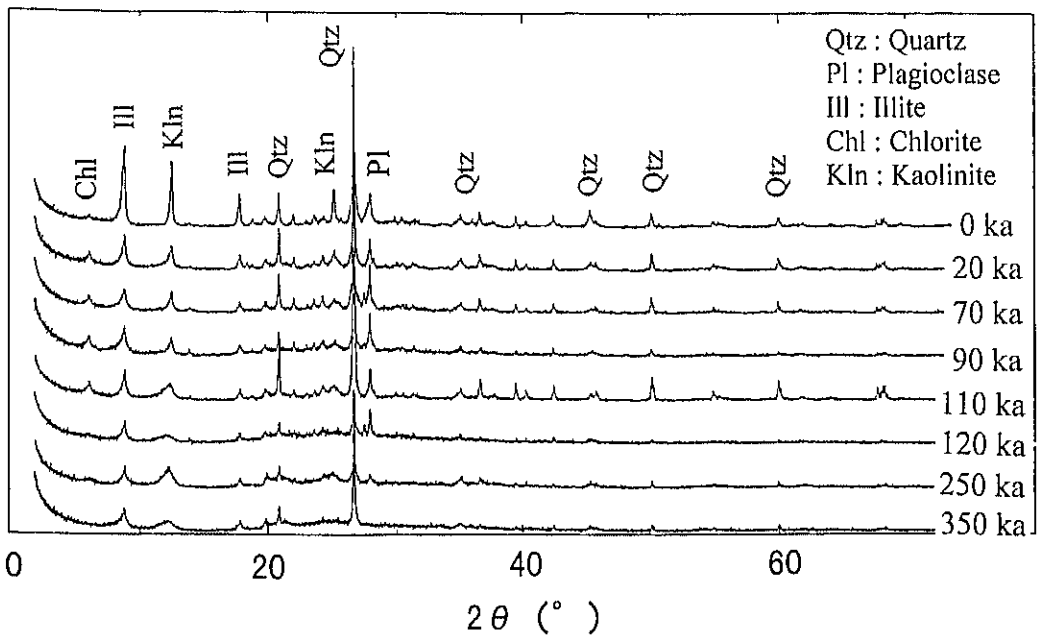

Fig. 8 X-ray diffraction patterns of matrix minerals in sandstone.

Mineral Compositions

Minerals were identified by X-ray diffraction analysis (XRD; Rigaku Co., Ltd., RAD-C System). The operating conditions included an X-ray target of CuK α, tube voltage of 50 kV and tube current of 20 mA. Matrix samples were analysed using three rock samples taken at each sampling site. The analysis followed the methods of Suzuki (1992) using silt size specimens in addition to treatments with ethylene-glycol.

The results of XRD are shown in Fig. 8. Samples include quartz, plagioclase and clay minerals such as kaolinite, chlorite and illite. Chlorite can be identified because the 2θ of diffracted pattern has not shifted after treatments with ethylene-glycol. The intensity of diffracted peaks of plagioclase, illite and kaolinite gradually decreased during 350 ka, while a diffracted peak of chlorite cannot be recognised after 250-ka rocks. These results show that plagioclase and clay minerals decompose as the weathering period increases.

Identification of Iron Minerals

The visible diffuse reflectance spectra of rocks and minerals have been used recently to characterise the origins of the colours of rocks (e.g., Nakashima et al., 1989, Matsunaka and Uwasawa, 1992; Nakashima, 1994; Hiroi, 1999; Kuchitsu et al., 1999; Sasaki and Otani, 1999). For example, iron minerals such as goethite and hematite can be identified by this technique.

Using about 20 pieces of gravel from each sampling site, visible diffuse reflectance spectra on the cutting surface of rock samples were measured using a Minolta CM-500 spectrophotometer in a visible wavelength region (400 to 700 nm). The measuring area was 3 mm in diameter. There are two kinds of reflection processes of light on solid materials: (1) that occurring when light is reflected from a polished surface of the mineral (specular reflection), and (2) that occurring when the light is reflected by the finely powdered mineral (diffuse reflection). The latter arises from radiation that has penetrated the crystals and reappeared at the surface after multiple

scatterings. When light is reflected from the rock surface, diffuse reflection occurs. If the intensity of the diffuse spectra reflectance light from the surface of a white plate ($BaSO_4$) is r_0 and that from the rock sample is r, the diffuse reflectance R is given by

$$R = r / r_0 \quad \cdots(1)$$

The results of the measurements are shown in Fig. 9. Reflectance spectra ranged from 8 to 42 %, increasing as the weathering period increases, while reflectance slightly decreases at 480 nm. As a significant trend from 90- to 250-ka rocks, increase at 500 to 600 nm. Reflectance for 350-ka rocks increases from 540 to 700 nm.

Nakashima et al. (1992) and Kuchitsu et al. (1999) have investigated in detail the visible reflectance spectra of iron minerals goethite (α-FeOOH), and hematite (α-Fe_2O_3). They have pointed out that the spectra of the two iron minerals show different patterns in the visible region: the reflectance of spectra of goethite increases in the 500- to 600-nm range and slightly decreases at 480 nm, and that of hematite increases at 540 to 700 nm. According to these previous studies, the reflectance spectrum of 90- to 250-ka rocks seems to be correspond to the spectra of goethite, and that of 350-ka rocks to the spectra of hematite. These findings suggest that iron minerals in the sandstone of the present study changes from goethite to hematite as the weathering period increases.

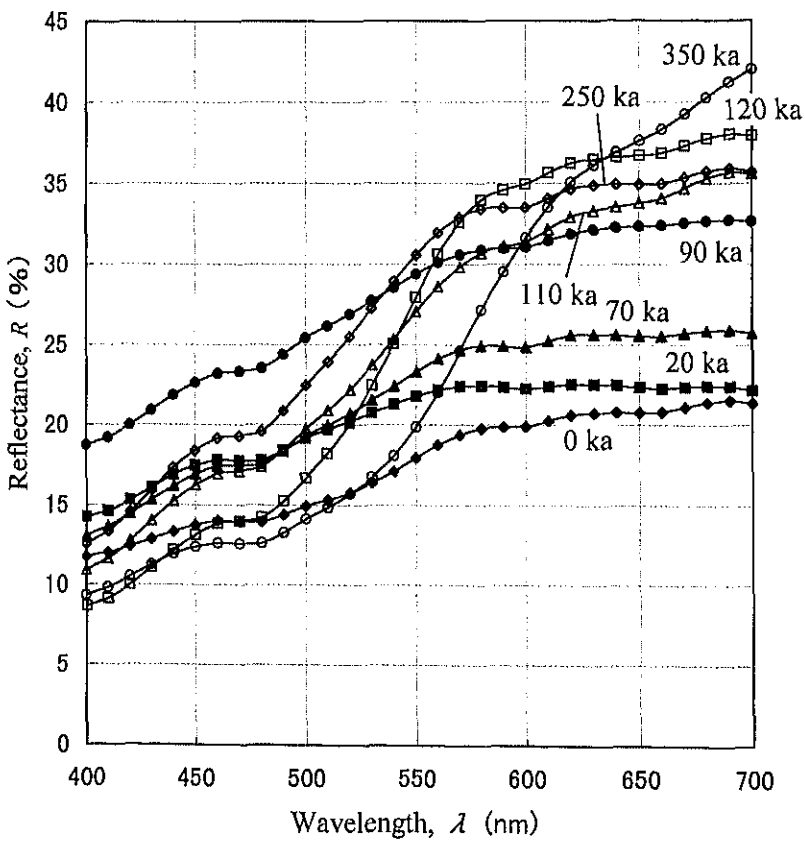

Fig. 9 Temporal changes in visible diffuse reflectance spectra.

Colour

Soil colour is closely related to the content of goethite and hematite (e.g., Torrent et al., 1983). Recent researchers in earth sciences have used a spectrophotometer to measure the colour of rocks, minerals and soils (e.g., Nagano and Nakashima, 1989; Nakashima et al., 1992; Nakashima, 1994; Oguchi et al., 1995; Ota and Kiya, 1996; Mitsushita et al., 1998; Wakizaka et al., 1998).

The colour of rock samples were determined using a Minolta CM-500 Spectrophotometer as having components L^*, a^* and b^*, i.e., L^* a^* b^* colour space. The L^*-value is the degree of lightness: $L^* = 0$ corresponds to black, and $L^* = 100$ corresponds to white. A positive value of a^* expresses red, and a negative value green. A positive value of b^* indicates yellow, and a negative value blue. Positive a^*- and b^*-values express an increase in iron minerals such as goethite and hematite (Nakashima et al., 1992; Nakashima, 1994). Colour measurements were carried out on a measuring line on a cutting surface of each rock sample at intervals of 5 mm using about 20 intact rock samples taken from each sampling site.

An example of colour measurements of the b^*-value is shown in Fig. 10. This figure shows that distributions of the b^*-value are almost uniform from the surface to the inner zone. Thus the mean value of all the measured values in each measuring line of individual rock samples is the representative colour value of each rock sample.

The results of colour measurements arranged by weathering time are shown in Fig. 11. The a^*-value ranges from −1.48 to 20.96, and the b^*-value ranges from −4.51 to 31.53. The a^*-value increases during the 250- to 350-ka period, and the b^*-value increases during the 0- to 250-ka period. These results support that the colour of rock samples becomes more yellowish during the 0- to 250-ka period and then more reddish during the 250- to 350-ka period.

The a^*-b^* diagram (Fig. 12) shows that the gradient of the trend line from plotted data is higher during the 0- to 250-ka period, while the gradient is gentle during the 250- to 350-ka period. Nakashima (1994) suggested that an increase in the b^*-value expressed an increase

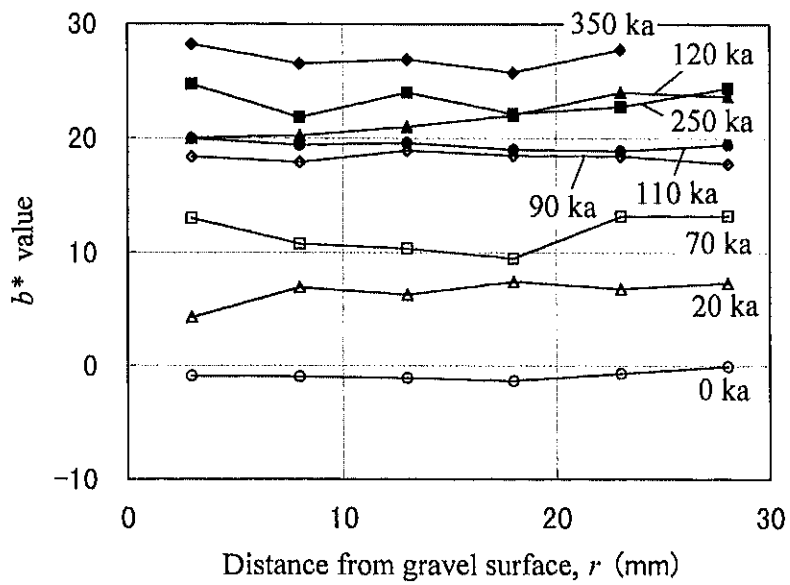

Fig. 10 Distribution of b*-value measured on cutting surface of gravel.

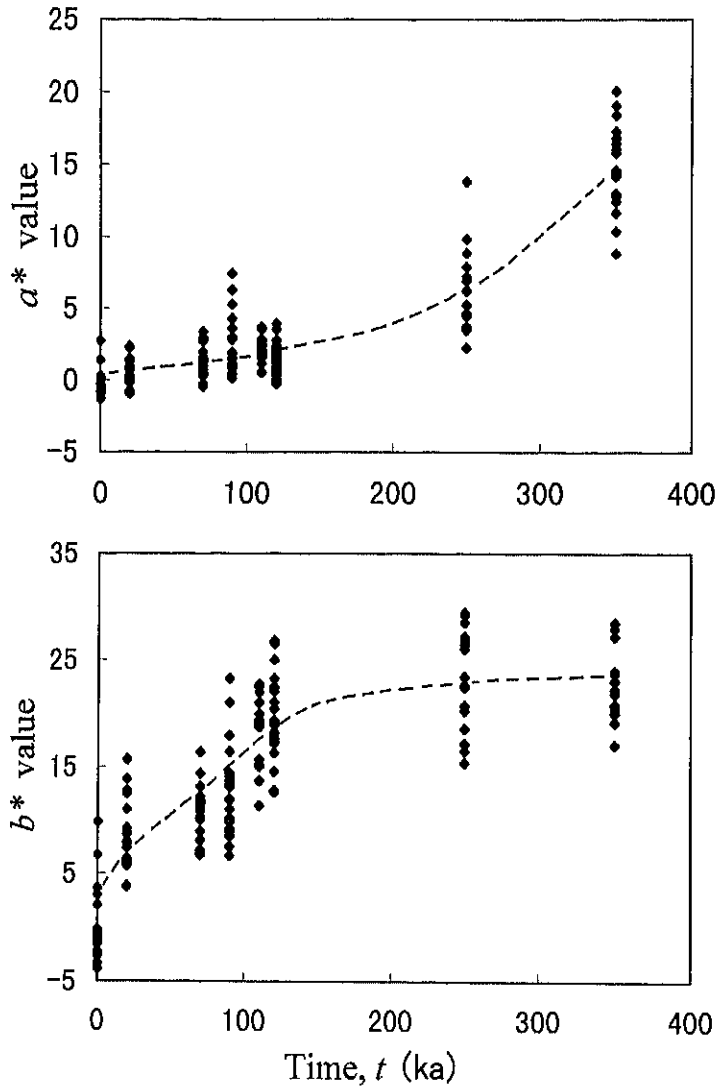

Fig. 11 Temporal changes in colour indices (a*- and b*- values).

in goethite and an increase in the a^*-value expressed an increase in hematite. Therefore, the present data of the a^*-b^* diagram indicate that goethite increases during the 0- to 250-ka period, and hematite increases during the 250- to 350-ka period.

Physical Properties

Effective Porosity and Apparent Specific Gravity

The effective porosity, n_e (%), and the apparent specific gravity, G_s, are widespread indices for physical properties of rocks. The methods of analysis were used by the Japanese Geotechnical Engineering Society (1989). The measurements were carried out using about 20 samples taken from each sampling site.

Temporal changes in the effective porosity and the apparent specific gravity are shown in Fig. 13. The effective porosity ranges from 0.75 to 30.19 %, and the apparent specific gravity ranges from 1.72 to 2.77. The effective porosity

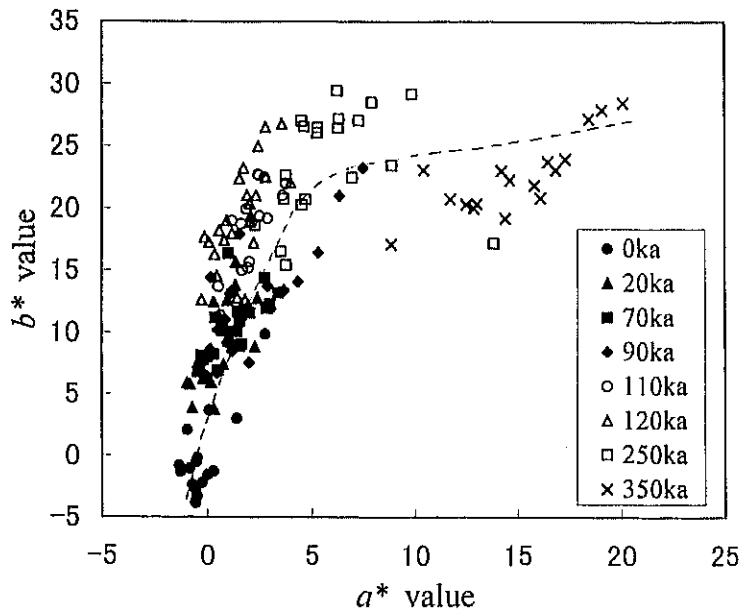

Fig. 12 Data plot on a*- b* diagram.

increases as the weathering period increases, while the specific gravity decreases during 350 ka. The effective porosity rapidly increases during 0 to 20 ka, and 90 to 120 ka, and after that a little increase in the n_e-value occurs during 120 to 350 ka. On the other hand, the apparent specific gravity rapidly decreases during 0 to 20 ka, and 90 to 120 ka, and its decreasing rate is slow during 120 to 350 ka.

Pore Size Distribution

Using three rock samples taken from each sampling site, pore-size distribution (PSD) was measured with a mercury intrusion porosimeter, the Porosimeter 2000 manufactured by the Karulo-Elva Co., Italy. The PSD of various rock types has been investigated in previous studies (e.g., Tamura and Suzuki, 1984; Uchino and Ichinose, 1984; Yamashita and Suzuki, 1986; Uchida and Tada, 1991,1992; Suzuki and Matsukura, 1992; Matsukura and Matsuoka, 1996; Oguchi and Matsukura, 1996; Tanaka et al., 1996; Lin and Takahashi, 1999; Lin et al., 1999; Takahashi et al., 1999). The method was devised by Washburn (1921), who assumed open pores with cylindrical shape. The pore diameter, d, is calculated by the following equation:

$$d = 4\gamma \cos\theta / P \quad \cdots(2)$$

where γ is the surface tension of mercury (484 dyne/cm), θ is the contact angle between mercury and solid (about 131°) and P is the pressure of mercury intrusion.

The significant range of PSD readings is from 3.3×10^{1} μm to 3.3×10^{-3} μm. Pores are tentatively divided into the following four ranges (Suzuki and Matsukura, 1992), d_a through d_d: large ($3.3\times10^{1}\geqq d_a > 3.3\times10^{0}$), medium ($3.3\times10^{0}\geqq d_b > 3.3\times10^{-1}$), small ($3.3\times10^{-1}\geqq d_c > 3.3\times10^{-2}$) and very small ($3.3\times10^{-2}\geqq d_d > 3.3\times10^{-3}$). Pore volumes per unit weight of rock samples are denoted as V_a, V_b, V_c and V_d (mm^3/g) for the four grades, respectively. The sum of V_a, V_b, V_c and V_d is called the total pore volume, V_{sum} (mm^3/g).

A representative example of the histogram of pore size distribution is shown in Fig. 14. The pattern of pore size distribution of 70- to 110-ka

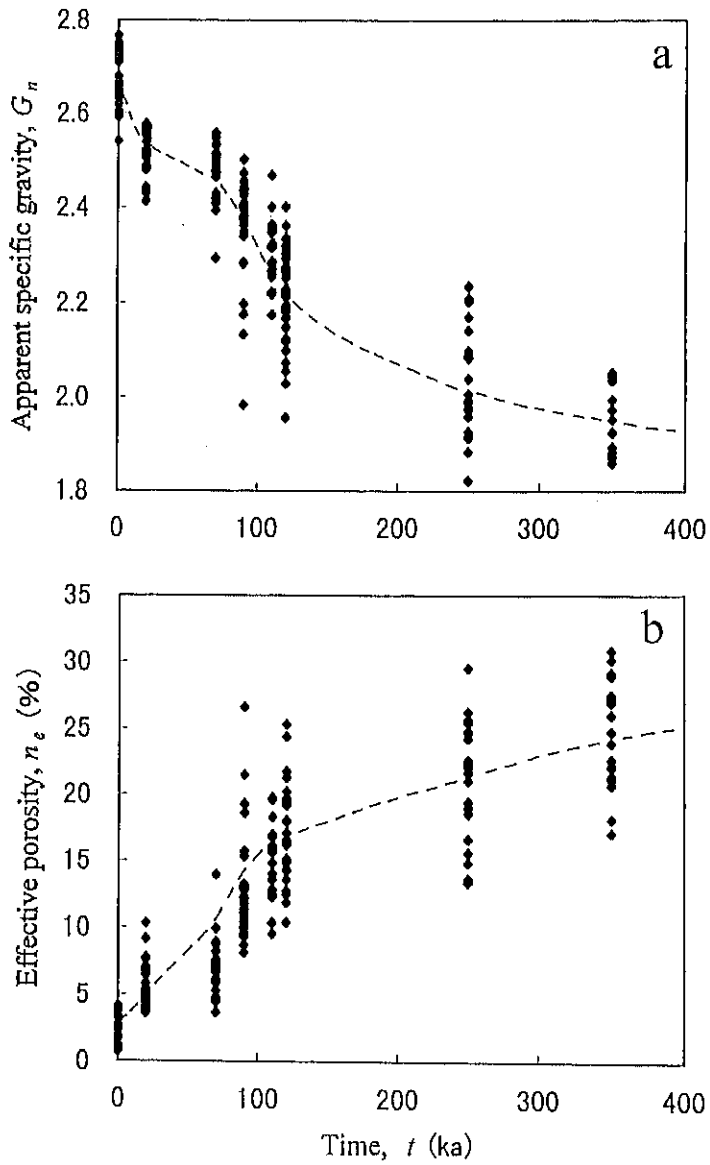

Fig. 13 Temporal changes in specific gravity, G_n (a), and effective porosity, n_e (b).

rocks mostly shows the normal distribution. In histograms for 120- to 350-ka rocks, the mode-value of pore volume is exceptionally rich. Both the mean pore radius and the total pore volume increase with increasing the weathering period.

Temporal changes in the pore volume fractions V_a, V_b, V_c and V_d are shown in Fig. 15. The values of V_a and V_b increase rapidly during the 120- to 350-ka period and during the 90- to 120-ka period, respectively. On the other hand, V_c and V_d increase only slightly as the weathering period increases. These facts show that the pore radius of sandstone increases as the weathering period increases, and increasing pore size is mostly more than 1 μm (V_a and V_b).

The mean pore radius, r (μm), and the specific surface area, S (m^2/g), were calculated from the pore size distribution data from each

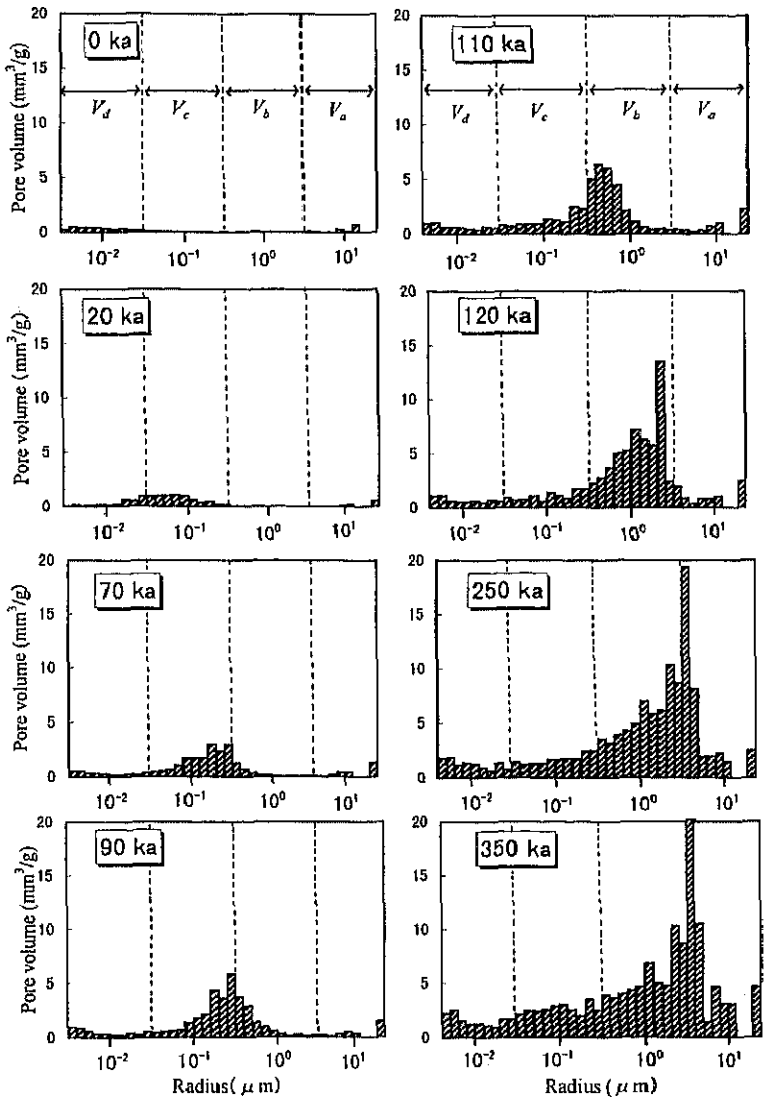

Fig. 14 Histograms of pore size distribution measured by the mercury intrusion porosimeter.

sample. The specific surface area, S, is calculated by the following equation:

$$S = -(1/M\,\gamma\cos\theta)\int PdV \quad \cdots (3)$$

where M is the mass weight, γ is the surface tension of mercury (484 dyne/cm), θ is the contact angle between mercury and solid (about 131°), P is the pressure of mercury intrusion, and V is the volume of mercury intrusion.

These results are shown in Fig. 16. The mean pore radius, r, ranges from 0.005 to 4.994 μm, and the specific surface area, S, ranges from 0.46 to 6.01 m^2/g. The mean pore radius increases as the weathering period increases, most rapidly during 90 to 120 ka. The specific surface area increases at a nearly constant rate during 350 ka. Thus the pore radius increases varying amounts, but the specific surface area increases at a constant rate as the weathering period increases.

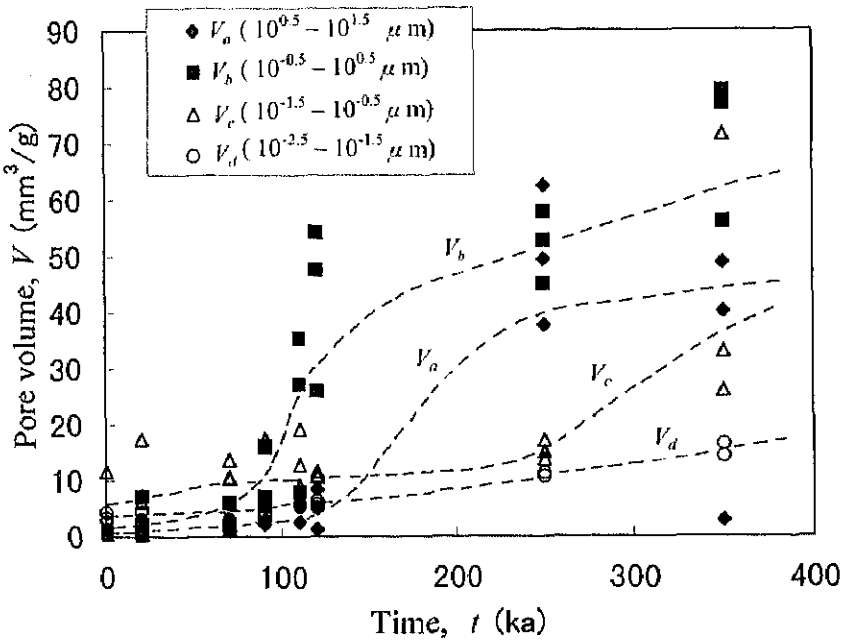

Fig. 15 Temporal changes in pore volume for four sub-ranges of pore size.

Permeability

The permeability of sandstone is usually measured by the transient pulse technique (e.g., Ishijima et al., 1991, 1993; Xue et al., 1992; Takahashi et al., 1993). This method uses a cylindrical test specimen. The gravel used for the present analysis is too hard to form into a cylindrical specimen because the pebbles are irregularly shaped and small. Therefore, the permeability was calculated using PSD data based on the hydraulic radius model (Peterson, 1983). Calculation was carried out by employing the method of Lin et al. (1999), which uses the following equation:

$$k = C_s \gamma \phi \{1/2[\Sigma f(r_i)/r_i]\}^{-2}/\mu \quad \cdots (4)$$

where k is the permeability (m/s), C_s is a constant value of 0.4, γ is the weight per unit volume, ϕ is the effective porosity, $f(r_i)$ is the frequency of pore size distribution, r_i is the capillary diameter (μm) and μ is the coefficient of viscosity (dyne · s · cm^{-2}, μ is 1 for water).

The results are shown in Fig. 17. The permeability of sandstone ranges from 10^{-11} to 10^{-7} m/s and increases as the weathering period increases. There was an especially rapid increase during 0 to 20 ka and 90 to 120 ka. After that, a small increase occurred during 120 to 350 ka.

Internal pore structure of rocks using X-ray CT

X-ray computed tomography analysis (X-ray CT), originally used for medical analysis, has been applied as a new non-destructive method of measuring internal density and pore structure of rock and soil samples (e.g., Raynaud et al., 1989; Nishizawa et al., 1995; Ikehara, 1997; Nakano et al., 1997, 2000; Sugawara et al., 1998, 1999; Duliu, 1999; Geet et al, 1999; Otani et al., 2000 a, b). An X-ray CT scanner generates a cross-sectional image through the rock samples by digitizing shadow pictures taken from various directions. The method is based on the measurements of the attenuation of the X-ray beam. For monochromatic radiation

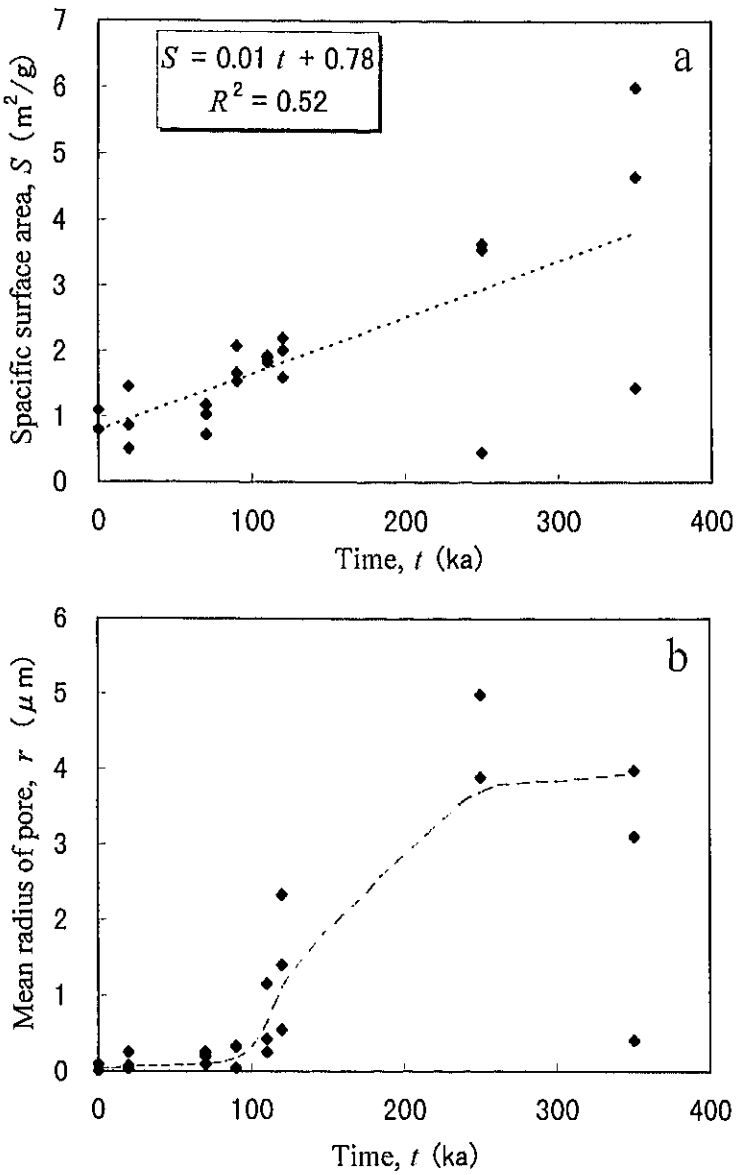

Fig. 16 Temporal changes in specific surface area, S (a), and mean pore radius, r (b).

of known intensity, I_0, across a homogeneous substance, the intensity, I, received after attenuation in the material is given by Lambert's Law (Raynaud et al., 1989), as follows:

$$I = I_0 e^{-\mu_i \rho x} \quad \cdots(5)$$

where μ_i is the absorption value per unit mass (cm^2/g), ρ is the density (g/cm^3) and x is the length of the material along the X-ray pass. Intensity I is converted to the CT-value using the following equations:

$$I = I_0 \exp(-U_{t\rho x}) \quad \cdots(6)$$
$$CT = K(U_t - U_w)/U_w \quad \cdots(7)$$

where U_t is the absorption value of the sample, U_w is the absorption value of water (0.171) and

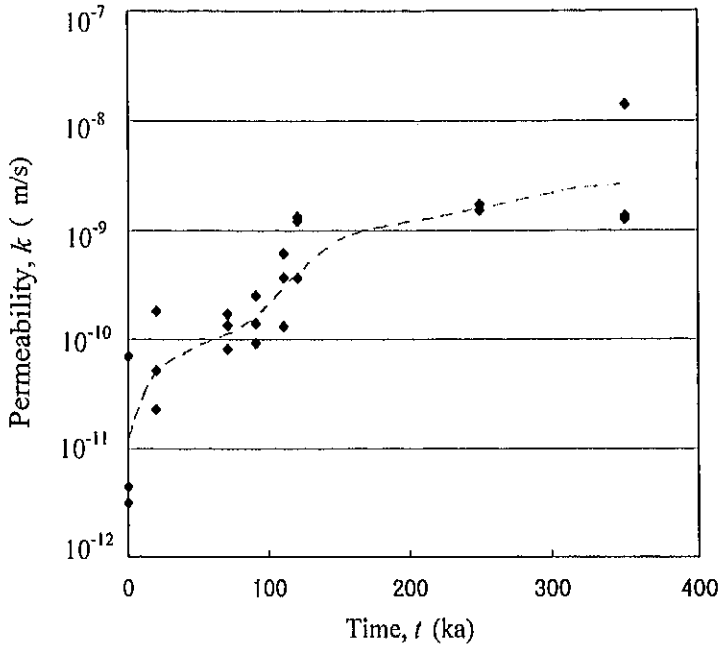

Fig. 17 Temporal changes in permeability using PSD data.

K is a constant of 1,000. The *CT*-value of water is zero. Since the absorption value of air is very small, 0.29×10^{-4}, the *CT*-value of air becomes $-1{,}000$. The *CT*-value depends mainly on material density reflecting pore structure.

Using 8 to 12 samples taken at each sampling site, X-ray CT images were measured with an X-ray CT scanner, a Toscanar 23200 mini manufactured by Toshiba Co., Japan, with 300-kV tube voltage and a 0.5-mm X-ray beam. The equipment can analyse a resolution area of less than 0.2×0.2 mm^2.

Representative CT images are shown in Fig. 18. The *CT*-value distribution of each sandstone is mostly uniform in the whole section of each type of gravel. Decreasing *CT*-value seems to indicate decreasing density (i.e., an increased porous zone). This shows that the distribution of pores in sandstone is uniform in the whole section of each specimen. Distribution of pores in the CT images is in good agreement with the result of microscope observation showing uniform pore distribution in thin sections (Fig. 7). Inner cracks are expressed as a low *CT*-value zone on CT images, as recognised in 120-ka rock (Fig. 18). X-ray CT analysis shows that no weathering rinds exist in most of the samples shown in Fig. 18. These results are in good agreement with the results of naked-eye observations of the cutting surfaces of rock samples (Fig. 6).

A rapid decrease in the mean *CT*-value as the weathering period increases can be noted on CT images of the period between 90- and 120-ka BP (Fig. 18). Figure 18 shows the detail of the changes in CT images of the sandstone between 90 and 120 ka. This figure shows that the *CT*-value rapidly decreases during the period 110 to 120 ka. In the CT images of 110-ka rock samples, the *CT*-value at the corner areas in the outer zone is higher than that of the inner zone. This phenomenon is considered to be a false image caused by the X-ray CT method itself (Nakano et al., 2000).

The average value of *CT*-value, denoted as CT_m, of each rock sample was calculated from the data of CT images. The results are shown in Fig. 19. The value of CT_m ranges from 779 to

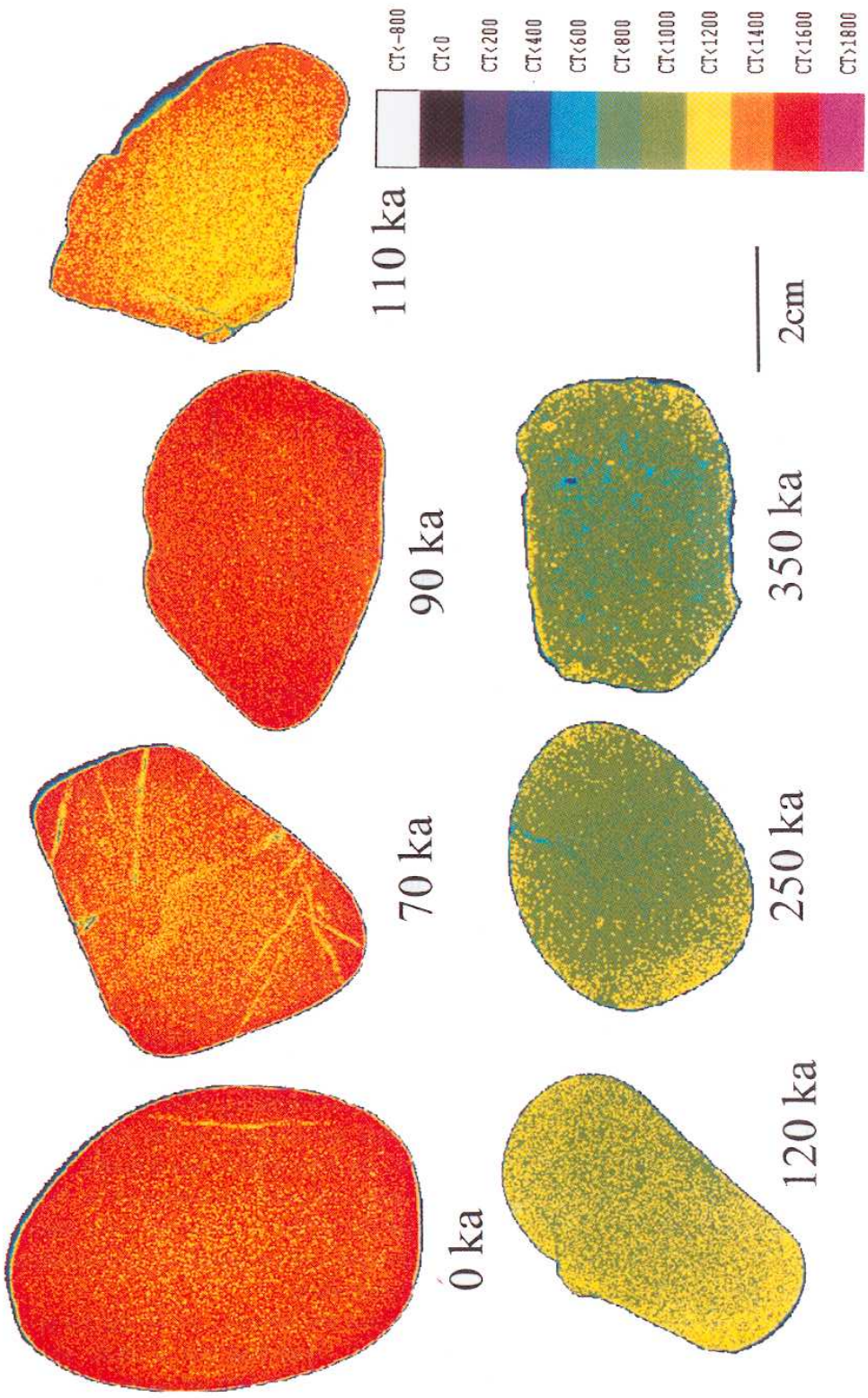

Fig. 18 Typical examples of X-ray CT images of sandstone gravel.

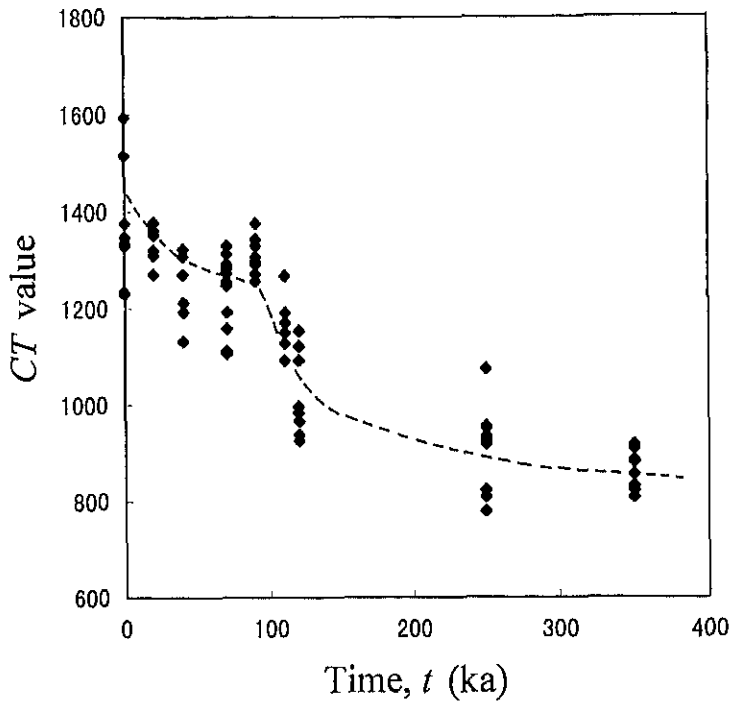

Fig. 19 Temporal changes in mean *CT* value, CT_m

1594 and follows a trend of decreasing as the weathering period increases, particularly during the 90- to 120-ka period. This finding indicates that sandstone pored increased during that period.

Chemical Properties

Chemical Composition using X-ray Florescence Analysis

Chemical composition of three rock samples taken from each sampling site was determined using X-ray florescence analysis (XRF: Rigaku model 3270). The following ten major elements were analysed: SiO_2, TiO_2, Al_2O_3, $FeO+Fe_2O_3$, MnO, MgO, CaO, Na_2O, K_2O and P_2O_5. Temporal changes in chemical compositions are shown in Fig. 20. Plotted data in this figure are limited to SiO_2, Al_2O_3, $FeO+Fe_2O_3$, MgO, CaO, Na_2O and K_2O.

Figure 20 shows that the chemical compositions of SiO_2, MgO, CaO, Na_2O and K_2O gradually decrease as the weathering period increases, while those of Al_2O_3 and $FeO+Fe_2O_3$ are mostly constant during 350 ka. Although SiO_2 is a compound with low solubility in natural water, it leaches out easily due to weathering. Alkali elements such as MgO, CaO, Na_2O and K_2O with high solubility also leach out easily due to weathering, while Al_2O_3 and $FeO+Fe_2O_3$ tend to remain in the internal part of gravel because both compounds have a low solubility. Quartz, plagioclase and clay minerals such as illite and kaolinite consist of silica. Decreasing silica is considered to be caused by leaching of clay minerals because they are more soluble than is quartz. Plagioclase consists of alkali elements such as Na_2O, K_2O and CaO. The decrease of these elements is considered to be caused by the decomposition of plagioclase.

Since the solubility of Al and Fe in natural water is lower than that of alkali elements, it remains in the matrix of sandstone. Aluminum is considered to be supplied by the

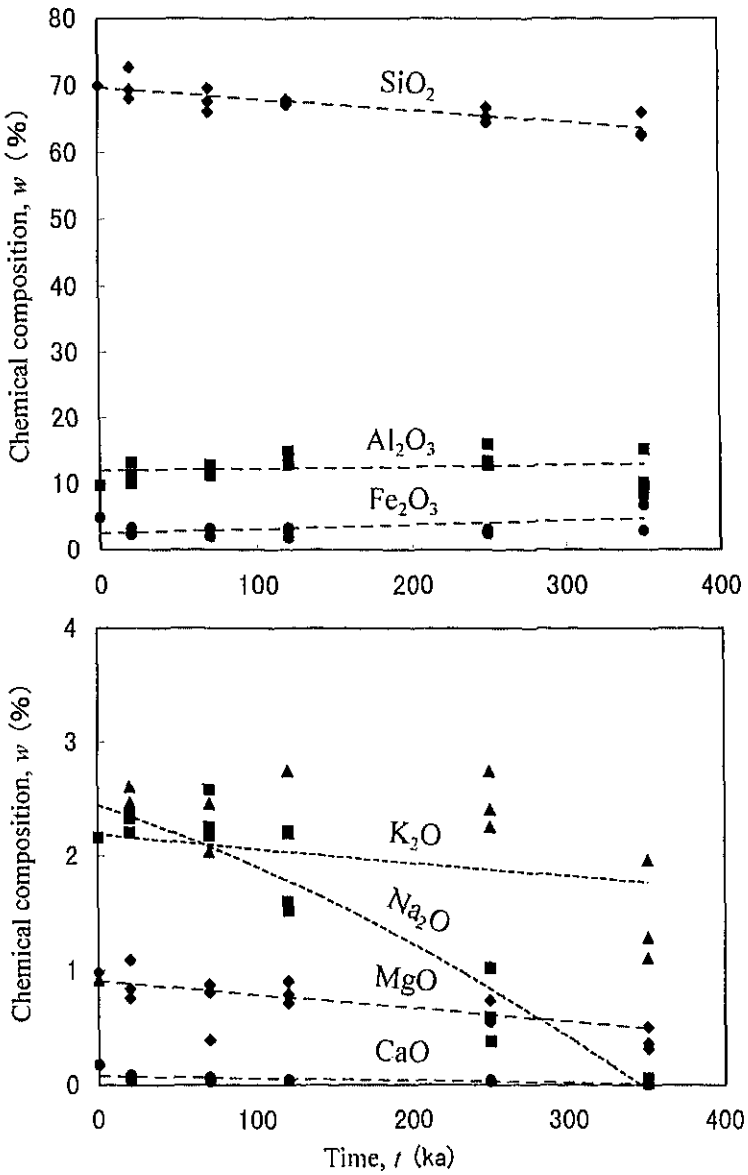

Fig. 20. Temporal changes in chemical compositions

decomposition of plagioclase, chlorite and kaolinite, and iron is considered to be supplied by the leaching of chlorite.

The *CIA*- and *PI*-values are excellent indices of leaching of chemical elements due to weathering (Reiche, 1943; Nesbitt and Young, 1982). *CIA*- and *PI*-values are calculated as follows:

$$CIA=100\times Al_2O_3/(Al_2O_3+Na_2O+K_2O+CaO) \quad \cdots(8)$$

$$PI=100\times SiO_2/(SiO_2+(FeO+Fe_2O_3)+Al_2O_3) \quad \cdots(9)$$

where Al_2O_3, Na_2O, K_2O, CaO, SiO_2 and $FeO+Fe_2O_3$ are given by weight %. The *CIA*-value expresses the degree of leaching of SiO_2, and the *PI*-value expresses the degree of

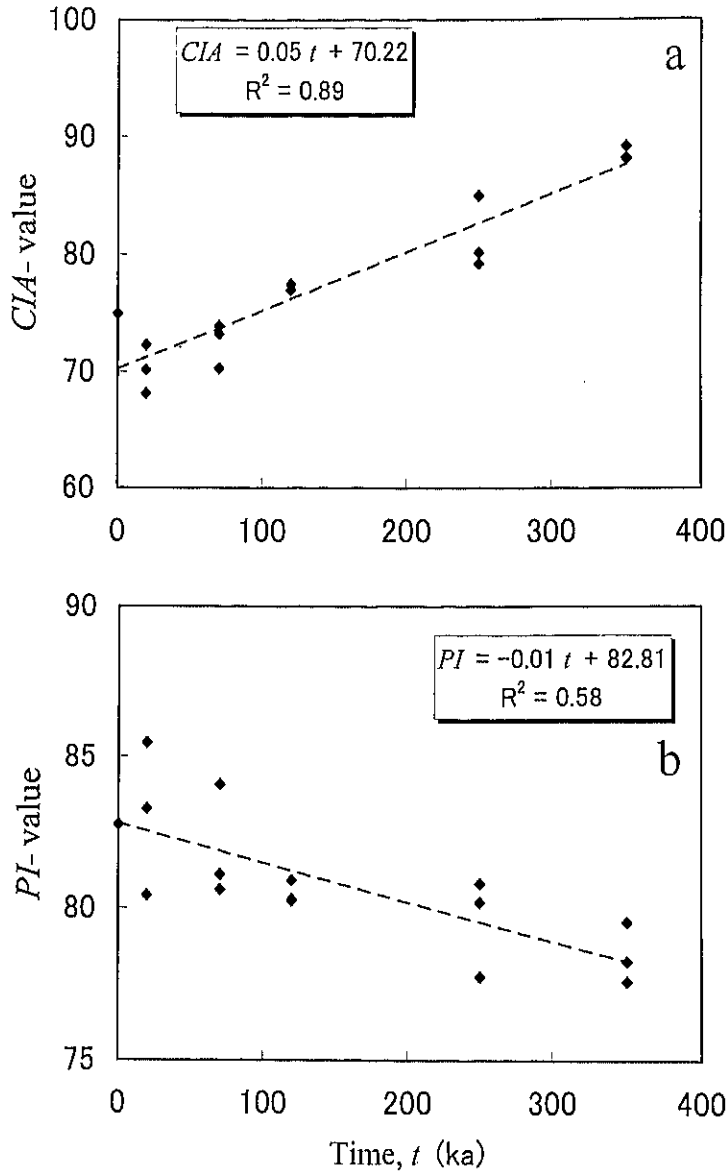

Fig. 21 Temporal changes in chemical weathering indices (*CIA*- and *PI*-values)

leaching of alkali elements (CaO, Na_2O and K_2O) because Al_2O_3 and $FeO+Fe_2O_3$ have a low solubility.

Temporal changes in the calculated *CIA*- and *PI*-values are shown in Fig. 21. The *CIA*-value ranges from 68.12 to 89.17, while *PI*-value ranges from 77.58 to 85.46. *CIA*- and *PI*-values change at a constant rate during 350 ka. Using the least squared fit method, the relationships between *CIA*-value and weathering period, t (ka), and *PI*-value and t are calculated as follows (R_2 is the contribution ratio):

$$CIA = 0.05\,t + 70.22,\ R^2 = 0.89 \quad \cdots(10)$$

$$PI = -0.01\,t + 82.81,\ R^2 = 0.58 \quad \cdots(11)$$

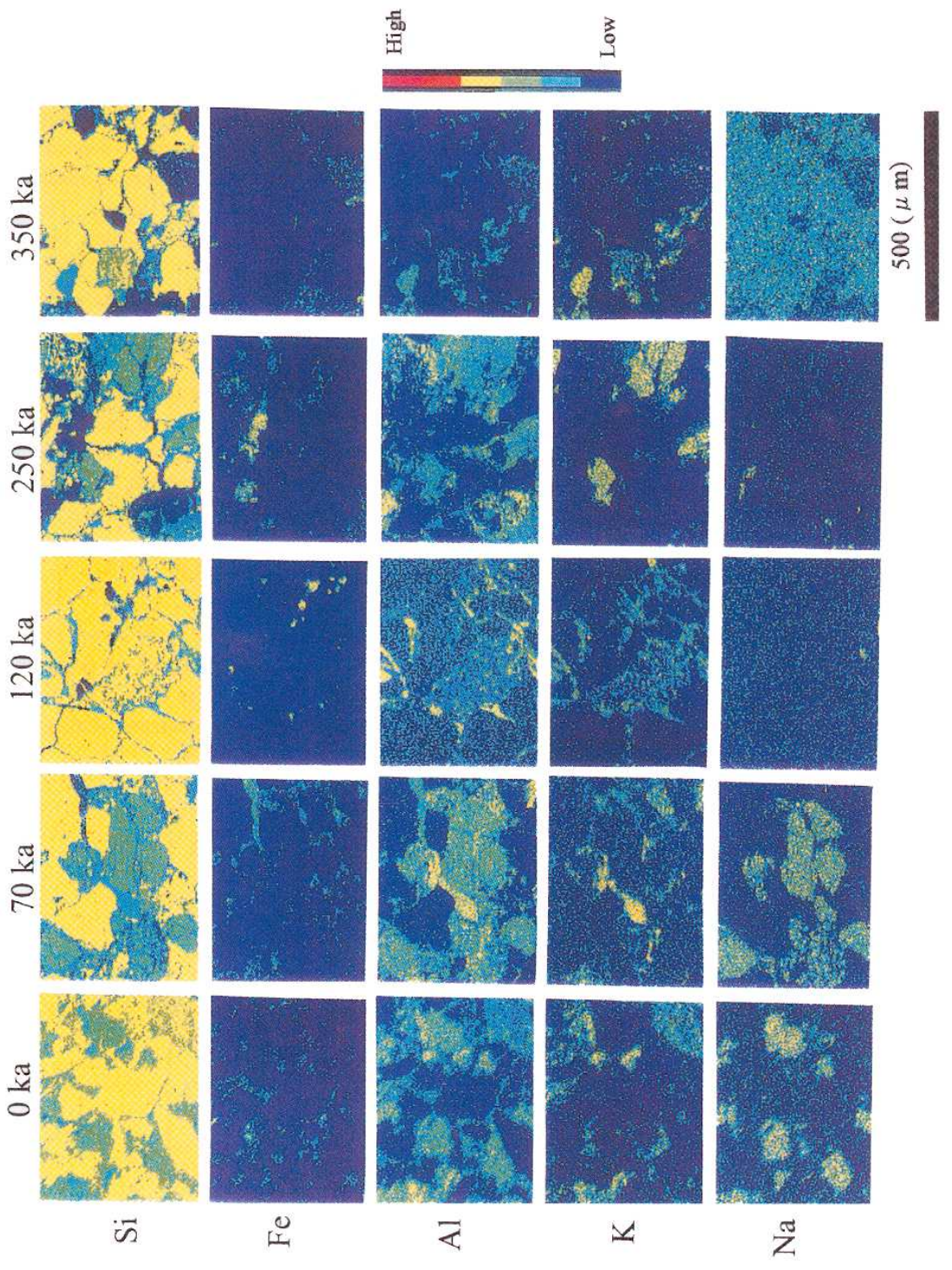

Fig. 22 Changes in Si, Fe, Al, K and Na concentrations constructed by EDS.

Distribution of Chemical Elements using Energy Dispersive X-ray Spectrometry

Energy dispersive X-ray spectrometry (EDS) was conducted to examine the concentration map of major elements in polished thin sections. Using three samples taken at each sampling site, the chemical mapping of Si, Fe, Al, K and Na was carried out.

The results of a concentration map of Si, Fe, Al, K and Na for 0-, 70-, 120-, 250- and 350-ka rocks are shown in Fig. 22. The EDS mapping images show that (1) the amount of Si in matrix decreases as the weathering period increases, and (2) the amount of K and Na in plagioclase decreases as the weathering period increases. A decrease of Si in matrix is considered to be caused by the leaching of clay minerals such as kaolinite, illite and chlorite. Decreases in the amount of K and Na are caused by leaching of plagioclase. The amount of Fe in matrix gradually concentrated during 350 ka. The amount of Al in matrix gradually concentrated during 0 to 250 ka, and after that the amount decreased during 250 to 350 ka.

Mechanical properties

The point loading tensile test (Hiramatsu et al., 1965) is a simple method for examining the mechanical properties of rocks. The strength of about 20 samples from each terrace deposit was measured with a point load strength apparatus (Model TS-40; Maruto Co., Japan). Tensile strength, σ_t (kgf/cm^2), is calculated by the following equation:

$$\sigma_t = 0.9F_0/d^2 \qquad \cdots(12)$$

where F_0 is load at failure (kgf), and d is the diameter of the rock sample at failure (cm). Point loading tensile strength was calculated to be the index of point load strength, τ, which is defined by Kimiya (1975 a) as follows:

$$\tau = \log \sigma_t \qquad \cdots(13)$$

Temporal changes in the τ are shown in Fig. 23. The σ_t ranges from 0.41 to 5400 (kgf), and the τ ranges from -0.39 to 3.48. This figure shows that the value of τ decreases during 0 to

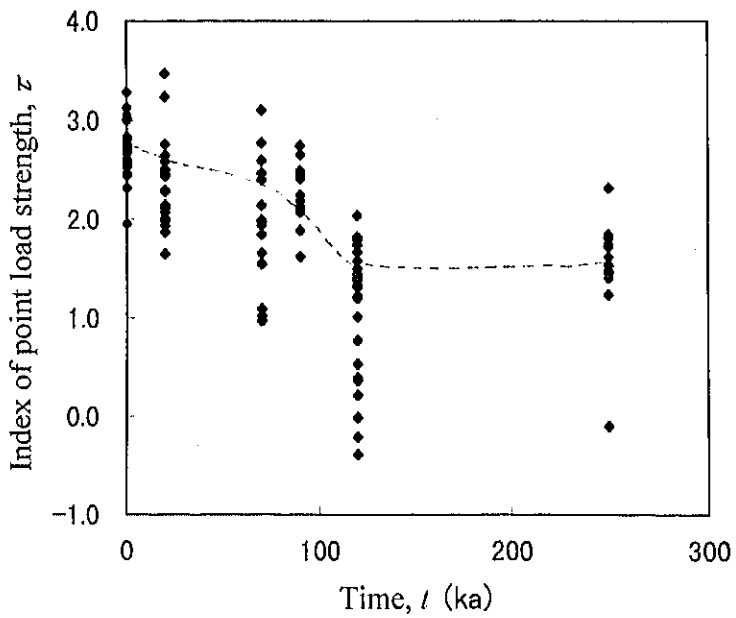

Fig. 23 Temporal changes in index of point load strength, τ.

120 ka, but after that the value of τ is constant during 120 to 250 ka. The rock strength decreases most rapidly during 90 to 120 ka.

Summary of the results

Figure 24 summarises temporal changes in the quantitative parameters, including colour, physical properties, chemical properties and mechanical properties. The average of the measured values in each rock property is plotted in this figure.

(1) *Changes in Colour*

Figure 24 shows that the a^*-value increases during the 250-to 350-ka period and the b^*-value increases during the 0- to 120-ka period, indicating that the colour of rock samples changes from grey to yellowish during 0 to 250 ka and subsequently changes to reddish during 250 to 350 ka. These results suggest that iron minerals in rock samples change from ferrihydrite to goethite during 0 to 250 ka and from ferrihydrite to hematite during 250 to 350 ka.

(2) *Changes in Physical Properties*

Effective porosity: Figure 24 shows that the effective porosity, n_e, increases as the weathering period increases. The effective porosity mostly increases during the 0- to 120-ka period, and after that a small increase in n_e occurs during the 120- to 350-ka period. This result shows that the volume of open pores rapidly increases during 0 to 120 ka.

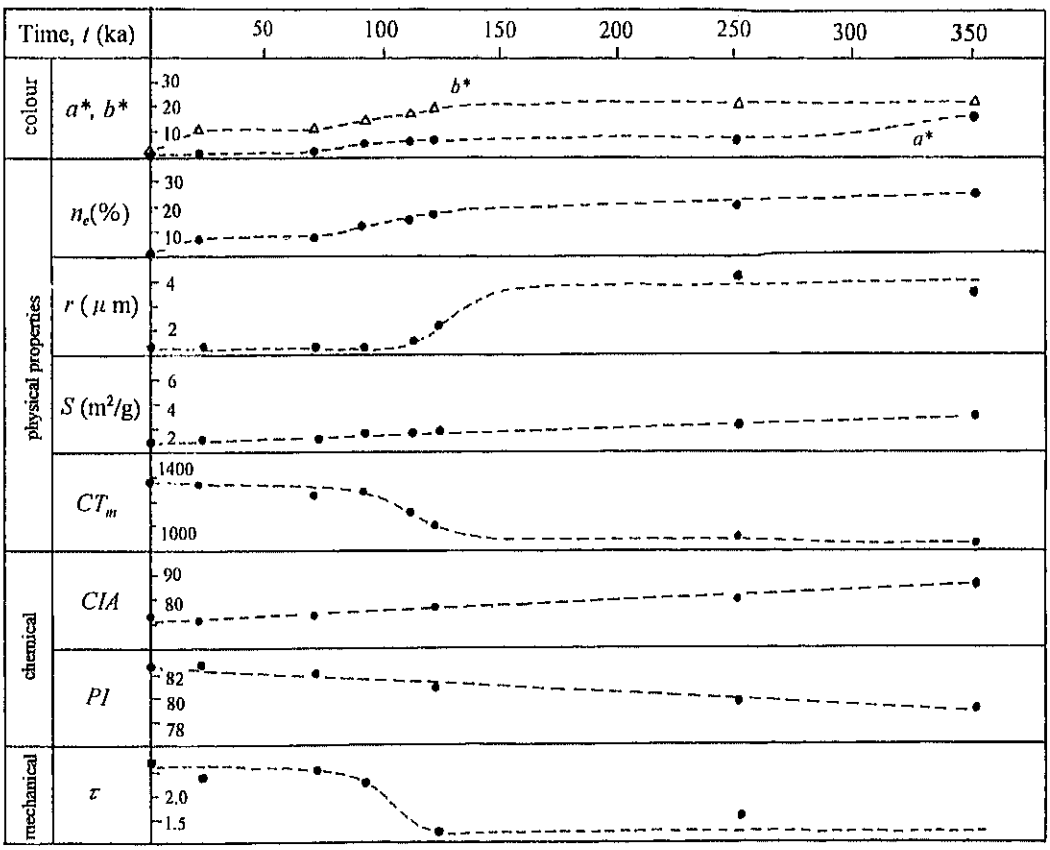

Fig. 24 An idealized diagram of temporal changes in rock properties.

Pore size distribution: Figure 15 shows that the pore volumes, V_c, and V_d, increase slightly as the weathering period increases, while V_b rapidly increases during 90 to 120 ka and V_a rapidly increases during 120 to 350 ka. This result shows that the pore radius of sandstone increases as the weathering period increases, but that enlargement occurs mainly in large pores more than 1 μm (V_a and V_b). As shown in Fig. 24, the mean pore radius, r, increases as the weathering period increases, particularly rapidly during 90 to 120 ka. On the other hand, the specific surface area, S, increases at a constant rate during 350 ka.

Internal pore structure of rocks using X-ray CT: Figure 24 shows that the CT_m-value decreases as the weathering period increases, and in particular it decreases rapidly during 90 to 120 ka. The latter supports the result that the pore radius of sandstone increases during 90 to 120 ka.

(3) *Changes in Chemical Properties*

Figure 20 shows that the chemical compositions of SiO_2, MgO, CaO, Na_2O and K_2O gradually decrease as the weathering period increases, while those of Al_2O_3 and $FeO+Fe_2O_3$ are mostly constant during 350 ka. This result shows that SiO_2 leaches easily due to weathering despite its low solubility. High-solubility compounds such as MgO, CaO, Na_2O and K_2O (consisting of alkali elements) also leach easily due to weathering, but Al_2O_3 and $FeO+Fe_2O_3$ tend to remain in the internal part of gravel because both compounds have low solubility. As in Fig. 24, the *CIA*-value increases and the *PI*-value decreases constantly as the weathering period increases. Thus, changing rates of chemical weathering are constant during 350 ka.

(4) *Changes in Mechanical Properties*

Figure 24 shows that the index of point load strength, τ, decreases during the 0- to 120-ka period, but after that it is constant during the 120- to 250-ka period. Rock strength decreases most rapidly during 90 to 120 ka.

DISCUSSION

Temporal Changes in Rock Properties

The temporal changes in rock properties due to weathering during 350 ka are examined using the above results. Patterns of temporal changes in rock properties shown in Fig. 24 can be subdivided into the following three types:

(Type-1): b*-value, effective porosity, n_e, mean pore radius, r, mean CT value, CT_m and index of point load strength, τ. These rock properties have high rates of changing during 90 to 120 ka, while they change only slightly during 0 to 90 ka and 120 to 350 ka.

(Type-2): a*-value. These rock properties change rapidly during 250 to 350 ka but only slightly during 0 to 250 ka.

(Type-3): Specific surface area, S, and two chemical weathering indices (*CIA*- and *PI*-values). These rock properties change constantly during 0 to 350 ka.

The Type-1 pattern includes physical properties except for the specific surface area, mechanical properties and the colour index of the b*-value: the patterns of temporal changes in physical and mechanical properties and the colour index of the b*-value are similar. The changing patterns of physical properties are similar to those of mechanical properties.

The physical properties and the colour indices change during the 0- to 120-ka period. The index of point load strength has decreased to the minimum value before 120 ka, i.e., rock strength first decreases in comparison to the other rock properties of Type-1. This result corresponds well to the results of previous studies (i.e., Oguchi et al., 1994). This relation suggests that rock strength is reduced by even slightly increasing pore volume and/or inner cracks.

The Type-2 pattern occurs only in the a*-value. The a*-value increases with increasing

the amount of hematite and degree of mineralization of hematite (e.g., Nakashima et al., 1992). The changes of iron minerals due to weathering are discussed in detail in later.

The Type-3 pattern includes the specific surface area and the chemical weathering indices (*CIA*- and *PI*-values). The changing rates of both indices are almost constant during 350 ka. This changing pattern suggests that chemical reactions occurred actively at the surface of the materials with a large specific surface area, as indicated by Oguchi et al. (1994). Since the specific surface area of sandstone increases at a constant rate during 350 ka, the chemical weathering indices change at a constant rate during 350 ka.

Temporal changes in rock properties of Type-1 accelerate during 90 to 120 ka. The period corresponds to the Last Interglacial Stage (Marine Isotope Stage 5; MIS 5) during 70- to 120-ka BP. The age of the maximum interglacial stage (MIS 5e) is estimated to be about 120-ka BP. Thus the rapid changes in these rock properties occurred during the Last Interglacial Stage (MIS 5). This agreement may suggest that a warm climate during the MIS 5 accelerated changes in rock properties. However, not all the rock properties changed rapidly during the MIS 5, and it is not clear that the relationships between changing rock properties were due to weathering and effects of changes of climate during the Quaternary.

Mechanism of Weathering in Sandstone Gravel

Change in Pore Structure in Sandstone due to Leaching of Matrix Minerals

The weathering mechanism of sandstone has been explained by increasing pore volume and pore radius caused by leaching of matrix minerals (e.g., Chigira and Sone, 1991). The primary pore geometry of sandstone has been examined in previous studies from the viewpoint of oil reservoir assessment in petroleum geology (e.g., Uchida and Tada, 1991). The pore geometry of sandstone is approximated to the skeleton network in previous studies (e.g., Scholle, 1979; Peterson, 1983; Doyen, 1988). For example, Doyen (1988) has constructed a model of pore structure that assumes that the distribution of pores and the pore radius are uniform throughout the whole rock.

Observations of photomicrographs (Fig. 7) and PSD data (Figs. 14 and 15) show that (1) connected and elongated pores with a diameter of 1 to 10 μm are mainly formed in matrix, and (2) micro-pores with a diameter of less than 1 μ m are rare. Observations of photomicrographs and CT images suggest that the distribution of pores is uniform throughout the whole gravel. The process of pore formation seems, therefore, to occur simultaneously throughout the gravel. This supports the field evidence that sandstone has no weathering rind.

The measurements of the effective porosity and pore-size distribution show that the pore volume and the mean pore radius of sandstone increase as the weathering period increases, as follows: (1) pore volume, V_p, and effective porosity, n_e, rapidly increased during 90 to 120 ka, as shown in Figs. 13 and 15, respectively, and (2) although V_a rapidly increased during 120 to 250 ka, n_e increased only slightly during 120 to 250 ka (Figs. 13 and 15). These changes are explained by the connection of pores that caused changes to the pore structure. For example, if neighboring pores running parallel are connected by leaching of matrix with each other, the V_{sum}-value would increase but effective porosity would remain constant. CT_m rapidly decreased during 110 to 120 ka (Fig. 19), which seems to have been caused by the increasing pore radius, not by the increasing pore volume.

The changing pattern of the *CT*-value corresponds to the changing pattern of V_p. On the other hand, the rate of change of the chemical weathering indices of sandstone is constant during 350 ka. The apparent

inconsistency of the changing pattern between the chemical weathering indices and the *CT*-value can be explained by the increase of connected pores. XRF data shows that there is no evidence of rapid leaching of chemical during the 90- to 120-ka period. The increased *r*-value and decreased *CT*-value seems to be caused by the degree of increased pore connection during the 90- to 120-ka period.

Some studies of the weathering of sandstone have been carried out (e.g., Chigira and Sone, 1991; Buntenuth et al., 1998;). Chigira and Sone (1991) noted that weathered tuffaceous sandstone is cemented by zeolite, and Buntenuth et al. (1998) wrote that the weathered sandstone they studied is cemented by silica gels. These both studies indicated that leaching of matrix minerals plays an important role in weathering of sandstone. It is well known that calcite, zeolite, silica gels and pyrite are easily dissolved. As described above, XRD results show that these minerals are not included in sandstone of the present study. In general, plagioclase changes into some kinds of clay minerals such as kaolinite due to weathering (e.g., Ollier, 1969). However, clay minerals and plagioclase monotonously decrease as the weathering period increases during 350 ka, and increasing clay minerals due to weathering cannot be recognised from the XRD results.

Chigira and Sone (1991) discussed that (1) concentrated iron minerals filled the pore space in matrix with weathering, and (2) decreasing in effective porosity and increasing in density occurred as a result of iron concentration. Photomicrographic observation and PSD data show that the effective porosity, n_e, increases as the weathering period increases (Figs. 7, 13 and 15), although iron minerals concentrate in the matrix of sandstone. Cementation of sand particles by iron minerals is not clear in sandstone gravel of the present study because rock strength decreases as the weathering period increases.

Although the pore volume and the pore radius increase as the weathering period increases, the specific surface area and the chemical weathering indices change at a constant rate during 350 ka. Microscope observation shows that the pores caused by leaching of matrix minerals are mostly straight and cylindrical in shape. The specific surface area of straight-like cylindrical pores seems to be small, even though the pores' radius is big. Characteristic properties of sandstone weathering are that (1) the pore radius increases as the weathering period increases, and (2) the changing rate of the specific surface area is constant. In general, chemical reaction occurred at the surface of the materials. Chemical weathering rates are constant because the increasing rate of the specific surface area is constant. Changing patterns of chemical weathering of rocks correspond to that of the specific surface area of rocks. The results of XRF data confirm that the rates of chemical weathering are constant.

The weathering mechanism of sandstone can be understood as the sequential leaching of matrix, as shown in Fig. 25. At the early stage of weathering, the porosity of sandstone is low because the matrix consists of clay minerals such as illite, kaolinite and chlorite. At the later stage of weathering, elongated and connected pores form in the matrix as a result of the leaching of clay minerals.

PSD data and the results of microscope observation show that geometrically, the pores are elongated and connected to each other. The structure of pores of the present study is similar to that of an elongate pore model described by Scholle (1977). The leaching of matrix in sandstone is mostly uniform in each of the whole rock samples. A weathering rind cannot be seen in the sandstone because of this uniform leaching that has occurred. The pore shape is also in accordance with the model of Doyen (1988). He suggests that the pore space morphology of sandstone is similar to the skeleton structure, having a network of

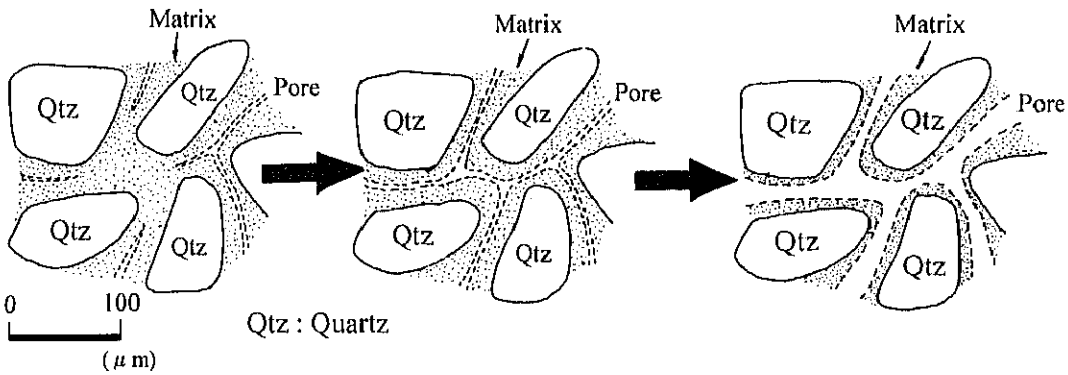

Fig. 25 Changes in pore structure of sandstone gravel.

cylindrical channels. In sandstone, cylindrical channels seem to be formed in matrix like those in the model shown in Fig. 25. In addition, the pore volume and the mean pore radius increase as the weathering period increases, and, thus, the radius of cylindrical channels seems to increase as the weathering period increases. To summarise, the leaching of matrix and the resulting increased pore volume play a major role in the weathering of sandstone.

Concentration of Iron Minerals in Matrix of Sandstone

The changing process of iron minerals due to weathering affects rock structure and changes in colour of sandstone. The results of observation of microphotographs show that iron minerals accumulated in matrix as the weathering period increased. Small amounts of iron minerals are found in 0- to 20-ka rocks, and the amounts increase in 70- to 350-ka rocks. Particles of iron minerals with a maximum diameter of 100 μm are recognised in 350-ka rock. In addition, the results of EDS show that Fe concentrates in matrix as the weathering period increases. In 0- to 70-ka rocks, the concentration of Fe is low over the whole thin section, while concentrated Fe particles form in 120- to 350-ka rocks in matrix, with a maximum diameter of as much as 100 μm. Fe^{2+} is formed by leaching of chlorite due to weathering. Fe^{2+} is easily oxidized to Fe^{3+} in an oxidative environment such as in terrace deposits. Fe^{3+} is precipitated within the rock because Fe^{3+} has a low solubility in natural water (e.g., Ichikuni, 1972). Hydroxides such as ferrihydrite are formed by precipitation of Fe^{3+}. The reaction of iron precipitation is expressed by the following equations:

$$Fe^{3+} + 3OH^- \rightarrow Fe(OH)_3 \downarrow \quad \cdots(14)$$

$$5Fe(OH)_3 \rightarrow Fe_5HO_8 \cdot 4H_2O + 3H_2O \quad \cdots(15)$$

where ferrihydrite ($Fe_5HO_8 \cdot 4H_2O$) is an amorphous mineral commonly recognised in red soils (e.g., Torrent et al., 1982, 1983; Schwertman and Murad, 1983, 1988; Campbell and Schwertman, 1984; Araki and Kyuma, 1987).

The colour of sandstone gravel changes to yellowish or reddish as the weathering period increases. The colour of rocks is affected by the iron minerals contained therein (Nakashima, 1994). For example, if hematite is added to powdered white almina by 0.77 and 0.05 weight percent, the powder changes to red and pink, respectively (Nakashima, 1994). This suggests that when sandstone becomes reddish due to weathering, it is caused by an increase in iron minerals such as hematite. The type of iron minerals could not be detected by XRD analysis of the sandstone because it has a relatively low iron mineral content. The results of colour measurement and spectroscopy analysis,

however, suggest that iron minerals in rock samples change from ferrihydrite to goethite (α-FeOOH) during the 0- to 250-ka period and from ferrihydrite to hematite (α-Fe_2O_3) during the 250- to 350-ka period.

Several studies have been carried out that examined the changing mechanism of iron minerals in red soils (e.g., Torrent et al., 1982, 1983; Schwertman and Murad, 1983, 1988; Campbell and Schwertman, 1984; Araki and Kyuma, 1987). Ferrihydrite could not be identified by XRD because it is amorphous mineral. Mizukami et al. (1999) have shown hydrogen-containing minerals in weathered sandstone using near infrared spectroscopy analysis. In addition, many amorphous iron minerals were included in red soils on the Higashibaru terrace in the Miyazaki Plain (Akagi et al, 1997). These hydrogen-containing minerals and amorphous iron minerals in the present study seem to be considered ferrihydrite.

Experimental studies of the dehydration of ferrihydrite have been carried out by Torrent et al. (1982) and Schwertmann and Murad (1983). These studies show that hematite increases at high temperature, low humidity and neutrality pH conditions, and goethite increases at low temperature, high humidity, and acidic and/or alkaric conditions. The formation process of goethite and hematite from ferrihydrite ($Fe_5HO_8 \cdot 4H_2O$) is discussed by Torrent et al. (1982). The results of this paper show that ferrihydrite can transform to hematite and goethite at high relative humidity, about 93 % (Torrent et al, 1982). When there is a lower relative humidity and a high temperature, the transformation to hematite is highly favored over transformation to goethite. These reactions are described by the following chemical equations:

$$2Fe_5HO_8 \cdot 4H_2O \rightarrow 5\,\alpha\text{-FeOOH} + 2H_2O \quad \cdots(16)$$

$$2Fe_5HO_8 \cdot 4H_2O \rightarrow 5\,\alpha\text{-}Fe_2O_3 + 5H_2O \quad \cdots(17)$$

The results of colour measurement and spectroscopic analysis show that goethite increased during 70- to 250-ka BP, and hematite increased during 250- to 350-ka BP (Figs. 9, 11, and 12). Although changes of iron minerals seem to be caused by changes in environmental conditions such as temperature and humidity at 250 ka, this contradicts the many studies concerning the Quaternary environmental changes. For example, as glacial-interglacial cycles are recognised in the Quaternary, drastic environmental changes around 250 ka contradict the above results. Because of this, changes in iron minerals cannot be explained by environmental changes that occurred around 250 ka. These considerations suggest that the formation of hematite required more time than that of goethite. The reaction in Eq. (16) seems to have occurred during the early stage of weathering, between 70 and 250 ka, and the reaction in Eq. (17) seems to have occurred

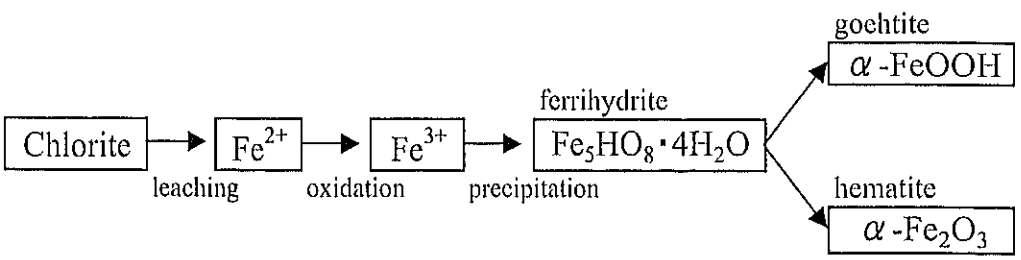

Fig. 26 Changes in Fe minerals of sandstone gravel.

during the later stage of weathering, between 250 and 350 ka.

The behavior and crystallization of iron in sandstone gravel due to weathering are summarised in Fig. 26. Iron originates from chlorite. Changing iron by oxidation, hydration and mineralization during weathering ultimately produces goethite and hematite. The rock structure and colour of sandstone gravel seem to be affected by changes of iron minerals in matrix.

CONCLUSIONS

Changes in several rock properties due to weathering have been investigated, and the weathering mechanism of sandstone has been clarified using sandstone gravel in dated terrace deposits whose formative ages are 0, 20, 70, 90, 110, 120, 250 and 350 ka. The following conclusions as illustrated in Fig. 27 can be drawn from this study:

(1) Although the appearance of quartz phenocrysts does not change as the weathering period increases, plagioclase has decomposed during 350 ka. Clay minerals in matrix also decomposed as the weathering period increased, while iron minerals have gradually concentrated in matrix during 350 ka.

(2) The a^*-value increased during 250 to 350 ka, and the b^*-value increased during 0 to 120 ka. This result suggests that iron minerals in rock samples changed from ferrihydrite to goethite between 0 and 250 ka and from ferrihydrite to hematite between 250 and 350 ka.

(3) Effective porosity increases as the weathering period increases. Pore volume indicators such as V_c, and V_d increased slightly as the weathering period increased, while V_b increased rapidly during 90 to 120 ka and V_a increased rapidly during 120 to 350 ka. These results show that the pore diameter of sandstone increases as the weathering period increases, and the increased pore size is mostly more than 1 μm (V_a and V_b). The mean pore diameter increases as the weathering period increases, particularly rapidly during the 90- to 120-ka period. On the other hand, the specific surface area increases at a constant rate during 350 ka. Observation of X-ray CT images shows that the distribution of pores in sandstone is uniform throughout each sandstone gravel.

(4) The chemical composition of SiO_2, MgO, CaO, Na_2O and K_2O gradually decreases as the

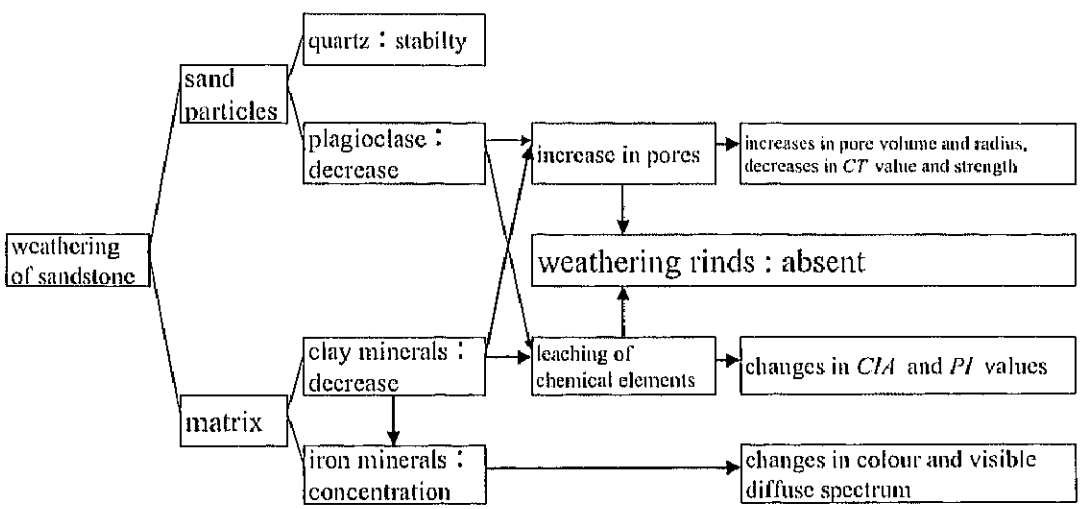

Fig. 27 General diagram of weathering mechanism of sandstone.

weathering period increases, while that of Al_2O_3 and $FeO+Fe_2O_3$ is mostly constant during 350 ka. These results show that SiO_2 is leached easily due to weathering, even though it has low solubility. Highly soluble compounds such as MgO, CaO, Na_2O and K_2O also leach easily due to weathering, but Al_2O_3 and $FeO+Fe_2O_3$ tend to remain in the internal part of gravel because both compounds have low solubility. The *CIA*-value increases and the *PI*-value decreases at constant rates as the weathering period increases. Thus rates of chemical weathering are constant during 350 ka.

(5) The index of point load strength decreases during 0 to 120 ka, but after that remains constant during 120 to 250 ka. In particular, rock strength decreases during 90 to 120 ka.

(6) The rock structure and colour of sandstone gravel seems to be affected by changes in the iron minerals in matrix. The behavior and crystallization of Fe due to weathering caused by oxidation, hydration and mineralization during weathering, which ultimately produces goethite and hematite.

(7) Weathering causes the leaching of matrix materials in sandstone, which increases pore volume and pore radius. In addition, pore volume and mean pore radius increase throughout gravel as the weathering period increases. These findings lead us to conclude that changes in the rock properties of sandstone due to weathering are the result of increased pore volume and the concentration of iron minerals in the sandstone matrix.

Acknowledgements

This research was conducted with supports from many people. I thank my Ph D supervisor, Professor Yukinori Matsukura, University of Tsukuba, for valuable discussion, guidance, and encouragement. Suggestions from Professor Eiji Matsumoto, Professor Masamu Aniya, Dr. Hiroshi Ikeda, Dr. Norikazu Matsuoka, Dr. Yuichi Onda, and Dr. Chiaki T. Oguchi, University of Tsukuba, are very helpful.

The experimental work would not have been possible without help from people in various institutes and universities. I am grateful to Dr. Katsuaki Koike, Kumamoto University, and Mr. Yosei Mizukami, National Space Development Agency of Japan, for measuring X-ray CT analysis. I am also grateful to Professor Seiji Takaya, Minami Kyushu University, and Dr. Shinji Nagaoka, Nagasaki University, Professor Yoshitaka Nagatomo, Miyazaki University, Mr. Yudzuru Inoue and Mr. Isao Akagi, Kagoshima University, Mr. Akira Shishido, Engineering geologist, and Mr. Kunihiro Yamamura, Komaki Co. Ltd and Masunaga Co. Ltd Joint venture, for their help with geological survey in the Miyazaki Plain. I thanks Professor Shozo Yokoyama and Professor Kazunori Watanabe, Kumamoto University, for their help of microscope observation of tephra. Chemical and mineralogical analyses were performed under assistance of Dr. Kosei Komuro, University of Tsukuba, and Dr. Tamao Hatta, Japan International Research Center for Agricultural Sciences. Measurements of pore-size distribution were performed under assistance of Dr. Manabu Takahashi, National Institute of Advanced Industrial Science and Technology, Dr. Weirin Lin, Dia Consultants Co. Ltd., and Xiaochun Li, Ibaraki University.

This research has been financially supported by Fukada Geological Institute in 1998-1999.

References

Akagi, I, Takaki, H. and Nagatomo, Y. (1997) Chemical composition of ferromagnetic minerals of the tephra deposits in the paleoredsoils on Miyazaki Coastal Plain. *Programme and abstract, Japan Assoc. Quat. Res.*, **27**, 212-213 (in Japanese).

Araki, S. and Kyuma, K. (1987) Weathering of Fe-Mg rich smectite in red soils developed on tuffaceous sandstone and andesite. *Soil Sci. Plant Nutr.*, **33**, 1-11.

Bell, F. (1978) The physical and mechanical properties of the fell sandstones,

Northumberland, England. *Engng. Geol.*, **12**, 1-29.

Bell, F. and Linsay, P. (1999) The petrographic and geomechanical properties of some sandstones from the newspaper member of the Natal Group near Durban, South Africa. *Engng. Geol.*, **53**, 57-81.

Butenuth, C., Fey, M., Freitas, M., Passas, N. and Forero-Duenas, C. (1998) Silica gels: a possible explanation for slope failures in certain rocks : *In* Maund, J. G. and Eddleston, M. eds., *Geohazards in Engineering Geology*, Geological Society, London, Engineering Geology Special Publications, **15**, 185-191.

Campbell, A. and Schwertman, U. (1984) Iron oxide mineralogy of placic horizons, *Jour. Soil Sci.*, **35**, 569-582.

Chigira, M. (1988) Weathering mechanism of sandstone (part 2) —weathering of fine-grained sandstone. *Abiko Research Laboratory Rep.* **U.88040**, 36p (in Japanese with English abstract).

Chigira, M. (1991) Chemical weathering mechanisms and their effects on engineering properties of soft sandstone and conglomerate cemented by zeolite in a mountainous area. *Engng. Geol.*, **30**, 195-219.

Chigira, M. and Sone, K. (1988) Weathering mechanism of sandstone (part 1) —weathering of coarse-grained sandstone cemented by zeolite. *Abiko Research Laboratory Rep.* **U.88039**, 32p (in Japanese with English abstract).

Crook, R. and Gillespie, A. (1986): Weathering rates in granitic boulders measured by P-wave speeds. In *Rates of Chemical Weathering of Rocks and Minerals* (eds., Colman, S. and Dethier, D.), Academic Press, Inc, pp.395-417.

Doyen, P. (1988) Permeability, conductivity, and pore geometry of sandstone. *Jour. Geophy. Res.*, **93**, 7729-7740.

Duliu, O. G. (1999) Computer axial tomography in geosciences: an overview. *Earth-Science Rev.*, **48**, 265-281.

Endo, H., and Suzuki, Y. (1986) *Geology of the Tsuna and Takanabe district, with geological sheet map at 1:50,000*, Geol. Surv. Japan. 105p (in Japanese with English abstract).

Endo, T. (1968) Geological study of the Miyazaki Coastal Plain, southeastern Kyushu, Japan. *Bull. Fac. Educ. Miyazaki Univ.*, **24**, 17-64.

Geet, M. V., Swennen, R. and Wevers, M. (2000) Quantitative analysis of reservoir rocks by microfocus X-ray computerised tomography. *Sedimentary Geol.*, **132**, 25-36.

Hachinohe, S., Hiraki, N. and Suzuki, T. (1999 a) Weathering rates of Tertiary sandstone and mudstone in Japan. *Z. Geomorph. N. F.*, **119**, 57-69.

Hachinohe, S., Hiraki, N. and Suzuki, T. (1999 b) Rates of weathering and temporal changes in strength of bedrock of marine terraces in Boso Peninsula, Japan. *Engng. Geol.*, **55**, 29-43.

Halsay, D. P. (1996) *The weathering of sandstone, with particular reference to buildings in the west Midlands, UK.* Wolverhampton University. 261p.

Hiramatsu, Y., Oka, Y. and Kiyama, H. (1965) Rapid determination of the tensile strength of rocks with irregular test pieces. *Jour. Mining. Metallurgical Institute Japan*, **81**, 1024-1030 (in Japanese with English abstract).

Hiroi, T. (1999) Quantitative analysis of rock-forming minerals by visible and near infrared remote sensing -silicate minerals as examples-. *Jour. Mineral. Soc. Japan*, **28**, 109-116 (in Japanese with English abstract).

Hirono, T. and Nakashima, S. (2000) Image visualization and quantitative analysis of void structure in sedimentary rock using image processing. *Jour. Geol. Soc. Japan*, **106**, 165-168.

Ichikuni, M. (1972) *Inorganic Geochemistry*, Baifuukan, Tokyo, 148p (in Japanese).

Ikehara, K. (1997) X-ray Computer Tomography: A nondestructive method for quantitative analysis of geological materials (part 1) - Instrument and imaging *Chishitsu News (Geological Survey of Japan)*, **516**, 50-61 (in Japanese).

Ishijima, Y., Xue, Z. and Takahashi, M. (1991) Permeability of the Neogene sedimentary rocks and its interpretation by using the equivalent channel model. *Jour. Japan Soc. Eng. Geol.*, **32**, 209-220 (in Japanese with English abstract).

Ishijima, Y., Xue, Z. and Takahashi, M. (1993) Some basic problems on measurements of hydraulic properties of rock by the transient pulse method. *Jour. Mining and Materials processing Inst. Japan*, **109**, 511-516 (in Japanese with English abstract).

Kimiya, K. (1975 a) Tensile strength as a physical scale of weathering in granitic rocks. *Jour. Geo. Soc. Japan*, **81**, 349-364 (in Japanese with English abstract).

Kimiya, K. (1975 b) Rates of weathering of gravels of granitic rocks in Mikawa and Tomikusa areas. *Jour. Geo. Soc. Japan*, **81**, 683-696 (in Japanese with English abstract).

Kimura, K., Iwaya, T., Mimura, K., Sato, Y., Sato, T., Suzuki, Y. and Sakamaki, Y. (1991) *Geology of the Osuzuyama district, with geological sheet map at 1:50,000*, Geol. Surv. Japan. 137p (in Japanese with English abstract).

Kino, Y., Kageyama, K., Okumura, K., Endo, H., Fukuta, O., and Yokoyama, S. (1984) *Geology of the Miyazaki district, Quadrangle series, scale 1:50,000*, Geol. Surv. Japan. 100p (in Japanese with English abstract).

Kuchitsu, N., Kuroki, N., Inokuchi, S. and Mitsuishi, S. (1999) Basic reserch on the reflectance spectra of mineral pigments. *HOZON-KAGAKU (Tokyo National Research Institute of Cultural Properties)*, **38**, 108-123 (in Japanese with English abstract).

Lin, W. and Takahashi, M. (1999) Permeability of Inada granite with high temperature history and its estimation by the equivalent channel models. *Jour. Japan Soc. Eng. Geol.*, **40**, 25-35 (in Japanese with English abstract).

Lin, W., Takahashi, M., Nishida, K. and Zhang, M. (1999) Equivalent channel models for permeability estimation and their application to sedimentary rocks. *Jour. Japan Soc. Eng. Geol.*, **39**, 533-539 (in Japanese with English abstract).

Machida, H. and Arai, F. (1992) *Atlas of tephra in and around Japan*. University of Tokyo Press, Tokyo, 276p (in Japanese).

Matsukura, Y. and Matsuoka, N. (1996) The effect of rock properties on rates of tafoni growth in coastal environment. *Z. Geomorph. N. F.*, **106**, 57-72.

Matsunaka, T. and Uwasawa, M. (1992) Near infrared diffuse reflectance spectra of clay minerals. *Soil Sci. Plant Nutri.*, **64**, 329-331 (in Japanese with English abstract).

Matsumoto, A. and Ui, T. (1997) K-Ar age of Ata pyroclastic flow deposits, southern Kyushu, Japan. *Bull. Volc. Soc. Japan*, **42**, 223-225 (in Japanese with English abstract).

Mitsushita, J., Ishizawa, K., Endo, T. and Takeuchi, T. (1998) Study for color measurement of rocks and its application to weathering classification and physical property evaluation. *Jour. Japan Soc. Eng. Geol.*, **38**, 370-385 (in Japanese with English abstract).

Mizukami, Y., Yoshinaga, T., Koike, K. and Nishiyama, K. (1999) Studies on rock weathering using X-ray CT and spectroradiometer. *Mining and material Processing Insti. Japan. Proc.*, 214-215 (in Japanese).

Nagano, T. and Nakashima, S. (1989) Study of colors and degrees of weathering of granitic rocks by visible diffuse reflectance spectroscopy. *Geochem. Jour.*, **23**, 75-83.

Nakano, T., Nakamura, K., Sometani, T. and Otsuka, H. (1997) Observation of 3-dimentional internal structure of rock using X-ray CT: (1) Density calibration of CT value. *Geoinfomatics*, **8**, 239-255 (in Japanese with English abstract).

Nakano, T., Nakashima, Y., Nakamura, K. and Ikeda, S. (2000) Observation and analysis of internal structure of rocks using X-ray CT. *Jour. Geol. Soc. Japan*, **106**, 363-378 (in Japanese with English abstract).

Nakashima, S. (1994) Colour change on the earth —Geochemistry of iron and uranium—. Kinmiraisya, Nagoya, 292p (in Japanese).

Nakashima, S., Ohki, S., and Ochiai, S. (1989) Infrared microspectroscopy analysis of the chemical state and distribution of hydrous species in minerals: *Geochem. Jour.*, **23**, 57-64.

Nakashima, S., Miyagi, I., Nakata, E., Sasaki, H., Nittono, S., Hirano, T., Sato, T., and Hayashi, H. (1992) Color measurement of some natural and synthetic minerals: *Rep. Res. Inst. Natural Resources, Mining College, Akita Univ.*, **57**, 57-76.

Nagaoka, S. (1984) Late Pleistocene tephrochronology in the region from the Osumi Peninsula to the Miyazaki Plain in the south Kyushu, Japan. *Jour. Geogr.*, **93**, 347-369 (in Japanese with English abstract).

Nagaoka, S. (1986) The landform evolution of the late Pleistocene in the Miyazaki Plain, south Kyushu, Japan. *Quat. Res.(Daiyonki Kenkyu)*, **25**, 139-163 (in Japanese with English abstract).

Nagaoka, S. and Arai, F. (1999) Quaternary tephrochronology and tectonics of Miyazaki Plain. *Proc. Asoc. Japan. Geograph.*, **55**, 350-351 (in Japanese).

Nagaoka, S., Arai, F., Nagatomo, Y., Akagi, I., Inoue, Y. and Nishiyama, K. (1998) Stratigraphy of Pleistocene marine sediments in Miyazaki Plain. *Programme and Abstracts, Japan Assoc. Quat. Res.*, **28**, 168-169 (in Japanese).

Nesbitt, H. W. and Young, G. M. (1982) Early proterozoic climates and plate motions inferred from major element chemistry of lutites. *Nature*, **299**, 715-717.

Nishiyama, K., Yokota, S. and Iwamatsu, A. (1999) Distribution and rock properties of reddish weathered gravels within the Quaternary fan deposits. *Jour. Japan Soc. Eng. Geol.*, **40**, 2-13 (in Japanese with English abstract).

Nishiyama, T., Kusuda, H., and Saito, T. (1992) A few remarks on examination of cavities or microcracks produced in rocks using a fluorescent substance. *Jour. Japan Soc. Eng. Geol.*, **33**, 17-22 (in Japanese with English abstract).

Nishizawa, O., Nakano, T., Noro, H. and Inazaki, T. (1995) Recent advances of X-ray CT technology for analyzing geologic materials. *Bull. Geol. Surv. Japan*, **46**, 565-571 (in Japanese with English abstract).

Oguchi, C. and Matsukura, Y. (1996) The change in microstructure of porous rhyolite due to weathering and its influence on the reduction of rock strength. *Trans. Japanese Geomor. Union*. **17**, 1-15 (in Japanese with English abstract).

Oguchi, C. and Matsukura, Y. (1999) Effect of porosity on the increase in weathering-rind thickness of andesite gravel. *Engng. Geol.*, **55**, 77-89.

Oguchi, C., Hatta, T. and Matsukura,Y. (1994) Changes in rock properties of porous rhyolite through 40,000 years in Kozu-shima Island, Japan. *Geogr. Rev. Japan*, **67A-11**, 775-793 (in Japanese with English abstract).

Oguchi, C., Hatta, T. and Matsukura, Y. (1999) Weathering rates over 40,000 years based on changing in rock properties of porous rhyolite. *Phys.Chem. Earth (A)*, **24**, 861-870.

Oguchi, C., Isobe, H., Komuro, K. and Matsukura, Y. (1995) Color measurements using a visible microspectrometer of weathering rinds on andesite blocks. *Ann. Rep. Inst. Geosci., Univ. Tsukuba*. **21**, 9-13.

Okada, H. (1977) Preliminary study of sandstones of the Shimanto Supergroup in Kyushu, with special reference to petrographic zone. *Sci. Rep. Dep. Geol. Kyushu Univ.*, **12**, 203-214 (in Japanese with English abstract).

Ota, T. and Kiya, H. (1997) Color changing of basic rock by artificial weathering. *Japan Soc. Eng. Geol. Proc.*, 117-120 (in Japanese).

Otani, J., Mukunoki, T. and Obara, Y. (2000 a) Application of X-ray CT method for characterization of failure in soils. *Soils and Foundations*, **40**, 111-118.

Otani, J., Obara, Y., Sugawara, K. and Mukunoki, T. (2000 b) Application of industrial X-ray computed tomography scanner to geotechnical engineering. *TSUCHI-TO-KISO (The Japanese Geotechnical Society)*, **48- 2**, 17-20 (in Japanese with English abstract).

Otsuka, Y. (1930 a) Geological problem of Takanabe district, Miyazaki prefecture. *Geogr. Rev. Japan*, **6**, 1048-1073 (in Japanese with English abstract).

Otsuka, Y. (1930 b) The crustal movement and the inclination of coastal terraces on the southeastern Kyushu. *Geogr. Rev. Japan*, **8**, 1-15 (in Japanese with English abstract).

Ollier, C. (1984) *Weathering (second edition)*. Longman London and New York., 270p.

Paichik, V. (1999) Influence of porosity and elastic modulus on uniaxial compressive strength in soft brittle porous sandstones. *Rock Mech. Rock Engng.*, **32**, 303-309.

Paterson, M. S. (1983) The equivalent channel model for permeability and resistivity in fluid saturated rock - A re-appraisal. *Mech. Materials*, **2**, 345-352.

Pentecost, A. (1991) The weathering rates of same sandstone cliffs, central Weald, England. *Earth Surf. Processes Landf.*, **16**, 83-91.

Raynaud, S., Fabre, D., Mazerolle, F., Greaud, Y. and Latiere, H. (1989) Analysis of the internal structure of rocks and characterization of mechanical deformation by a non-destructive method: X-ray tomodensitometry. *Tectonophysics*, **159**, 149-159.

Reiche, P. (1943) Graphic representation of chemical weathering. *Jour. Sediment. Petrol.*, **13**, 58-68.

Sasaki, Y. and Otani, T. (1999) Development of a visible and near infrared multi-spectrograph, and its utilization for estimation of strength and type of rocks. *Japan Soc. Eng. Geol. Proc.*, 195-198 (in Japanese).

Scholle, P. (1979) *A color illustrated guide to constituents, textures, cements, and porosities of sandstone and associated rocks*. The American Association of Petroleum Geologists, Oklahoma, 201p.

Schwertman, U. and Murad, E. (1983) Effect of pH on the formation of goethite and hematite from ferrihydrite. *Clays and Clay Minerals*, **31**, 277-284.

Schwertman, U. and Murad, E. (1988) The nature of an iron oxide -organic iron association in a peaty environment. *Clay Minerals*, **23**, 291-299.

Sugawara, K., Kojima, R., Obara, Y., Sato, A. and Shimada, H. (1998) Crack opening analysis by means of the X-rays CT. *Jour. Mining and Materials Processing Inst. Japan*, **114**, 881-887 (in Japanese with English abstract).

Sugawara, K., Sato, A., Obara, Y. and Yanagisako, M. (1999) Measurement of permeability of rock by means of X-ray CT. *Jour. Mining and Materials Processing Inst. Japan*, **115**, 803-808 (in Japanese with English abstract).

Suzuki, S. (1992) Paleoenvironment of the ultra-Tamba zone by means of modal and chemical compositions of sandstone. *Mem. Geol. Soc. Japan*, **38**, 71-83 (in Japanese with English abstract).

Suzuki, T. and Hachinohe, S. (1995) Weathering rates of bedrock forming marine terraces in Boso peninsula, Japan. *Trans. Japan. Geomorph. Union*, **16**, 93-113.

Suzuki, T. and Matsukura, Y. (1992) Pore-size distribution of loess from the loess plateau, China. *Trans. Japan. Geomorpho. Union*, **13**, 169-183.

Suzuki, K. and Takahashi, M. (1994) A visualizing method of pores and cracks using filmy replica system. *Jour. Japan Soc. Eng. Geol.*, **35**, 77-78 (in Japanese with English abstract).

Takahashi, M., Lin, W., Nishida, K. and Zhang, M. (1999) Measurement of pore size distribution in rocks by mercury intrusion porosimeter. *TSUCHI-TO-KISO (The Japanese Geotechnical Society)*, **47-4**, 30-32 (in Japanese with English abstract).

Takahashi, M., Sugita, Y., Xue, Z., Oonishi, Y. and Ishijima, Y. (1993) Three principal stress effects on permeability of the Shirahama

sandstone. *Jour. Mining and Materials Processing Inst. Japan*, **109**, 803-809 (in Japanese with English abstract).

Takahashi, M., Xue, Z., Oowada, A. and Ishijima, Y. (1992) On the study of interconnected pore network using a blue dyed epoxy impregnated thin section. *Jour. Japan Soc. Eng. Geol.*, **33**, 294-306 (in Japanese with English abstract).

Tamura, H. and Suzuki, T. (1984) Pore size distribution and other physical properties of Tertiary sedimentary rocks. *Trans. Japan. Geomor. Union*, **5**, 311-328 (in Japanese with English abstract).

Tanaka, Y., Hachinohe, S. and Matsukura, Y. (1996) The influence of slaking susceptibility of rocks on the formation of Hoodoos in Drumheller badlands, Alberta, Canada. *Trans. Japan. Geomorph. Union*, **17**, 107-121.

Teraoka, Y. (1977) Comparison of the Cretaceous sandstones between the Shimanto Terrene and the median zone of Southwest Japan, with reference to the provenance of the Shimanto geosynclinical sediments. *Jour. Geol. Soc. Japan*, **83**, 795-810 (in Japanese with English abstract).

Teraoka, Y. (1979) Provenance of the Shimanto geosynclinical sediments inferred from sandstone compositions. *Jour. Geol. Soc. Japan*, **85**, 753-769 (in Japanese with English abstract).

Teraoka, Y., Okumura, K., Suzuki, M. and Kawakami, K (1999) Clastic sediments of the Shimanto Supergroup in Southwest Japan. *Bull. Geol. Surv. Japan*, **50**, 559-590 (in Japanese with English abstract).

Teraoka, Y., Suzuki, M., Hayashi, T. and Okumura K. (1995) Stratigraphical variation in chemical composition of sedimentary rocks in the Shimanto Supergroup of the Makinime - Mikado area, East Kyushu, Southwest Japan. *Bull. Fac. Educ. Hiroshima Univ., Part II*, **17**, 83-94 (in Japanese with English abstract).

The Japanese Geotechnical Society (1989) *GAN-NO-CYOUSA-TO-SHIKEN (Field survey and test of rocks)*, 371-377 (in Japanese).

Torrent, J., Guzman, R. and Parra, M. (1982) Influence of relative humidity on the crystallization of Fe (III) oxides from ferrihydrite. *Clays and Clay Minerals*, **30**, 337-340.

Torrent, J., Schwerman, U., Fechter, H. and Alfrez, F. (1983) Quantitative relationships between soil color and hematite content. *Soil Science*, **136**, 354-358.

Tungrul, A. and Zarif, I. (1998) The influence of mineralogical, textural and chemical characteristics on the durability of selected sandstones in Istanbul, Turkey. *Bull. Int. Asoc. Eng. Geol. Env.*, **57**, 185-190.

Uchida, T. and Tada, R. (1991) Pore properties of sandstone - Part 1. Experimental investigation-. *Jour. Japan Assoc. Petroleum Tech.*, **56**, 387-399 (in Japanese with English abstract).

Uchida, T. and Tada, R. (1992) Pore properties of sandstone - Part 2. Application of pore-size distribution to natural sandstone-. *Jour. Japan Assoc. Petroleum Tech.*, **57**, 213-222 (in Japanese with English abstract).

Uchino, K. and Ichinose, M. (1984) Investigation of pore structure of coal measure rocks. *Jour. Japan Soc. Eng. Geol.*, **25**, 195-205 (in Japanese with English abstract).

Ulusay, R., Tureli, K. and Ider, M. (1994) Prediction of engineering properties of a selected litharenite sandstone from its petrographic characteristics using correlation and multivariate statistical techniques. *Engng. Geol.*, **37**, 135-157.

Wakizaka, Y., Ohara, M., Takahashi, T., Furuichi, H., Harada, M. and Tanaka, M. (1998) Mineralogical and chemical properties of clays for discrimination of weak zone type: *8th Congr. Inter. Assoc. Engng. Geol. Environm.*, Vol. I, 359-367.

Washburn, E. (1921) Note on a method of determining the distribution of pore sizes in a porous material. *Proc. National Academy of sciences*, **7**, 115-116.

White, K., Bryant, R. and Drake, N. (1998) Techniques for measuring rock weathering:

application to a dated fan segment sequence in southern Tunisia. *Earth Surf. Processes Landf.*, **23**, 1031-1043.

Xue, Z., Ishijima, Y. and Takahashi, M. (1992) Permeability and microgeometry of sandstone under hydrostatic pressure. *Jour. Mining and Materials processing Inst. Japan*, **108**, 769-775 (in Japanese with English abstract).

Yamashita, S. and Suzuki, T. (1986) Changes in pore-size distribution of sedimentary rocks due to weathering and the resultant decrease in their strength. *Trans. Japan. Geomor. Union*, **7**, 257-273 (in Japanese with English abstract).

Yusa, Y., Arai, T., Kamei, G. and Takano, H. (1991) Natural analogue study on long-term leaching behavior of radioactive waste glass: weathering alteration of volcanic glasses from Fuji and Izu-Ohshima volcanoes, Japan. *Jour. Atomic Power Soc. Japan*, **33**, 890-905 (in Japanese with English abstract).